A STUDY OF THE CONVECTIVE STORMS OF 14 MAY 1970 USING DATA FROM THE NSSL RAWINSONDE MESONETWORK

by

JACK M. MENEELY

S.B., Massachusetts Institute of Technology
(1965)

SUBMITTED IN
PARTIAL FULFILLMENT
OF THE REQUIREMENTS FOR THE
DEGREE OF MASTER OF SCIENCE
at the
MASSACHUSETTS INSTITUTE OF
TECHNOLOGY

June, 1972

Signature of Author _____
Department of Meteorology, May 11, 1972

Certified by _____
Thesis Supervisor

Accepted by _____
Chairman, Departmental Committee
on Graduate Students

A Study of the Convective Storms of 14 May 1970 Using Data From the NSSL Rawinsonde Mesonetwork

by

Jack M. Meneely

Submitted to the Department of Meteorology on 11 May 1972 in partial fulfillment of the requirements for the degree of Master of Science

Abstract

Data have been analyzed for the portion of a well-developed line of convective storms which moved through the NSSL mesonetwork. The storms occurred 10 to 15 nm behind the leading edge of a shallow layer of advancing cold air and formed a very narrow line of closely-spaced cells. Within the 4000-km^2 NSSL network, 58 rawinsonde ascents were made in a seven-hour period. The data from these soundings have been combined and averaged to describe the mesoscale, two-dimensional, transverse distribution of meteorological variables in the system. These results have been related to the data taken at 44 automatic recording surface stations.

A major backing of the mid-tropospheric winds occurred throughout the network while the system was within it, and lasted only a few hours. This phenomenon, attributed to a strengthening of the ageostrophic frontal circulation, had a major effect on the character of the storm system. Examination of the continuous PPI radar coverage showed that virtually all of the individual cells moved to the right of the environment winds, but the major contribution to the average motion of the storm line was the generation of new cells along its leading edge. Occasionally a complete and dramatic redevelopment of the storm line occurred well ahead of its former position. One instance of this is examined in some detail.

Thesis Supervisor: Frederick Sanders
Title: Professor of Meteorology

TABLE OF CONTENTS

LIST OF TABLES

LIST OF ILLUSTRATIONS

1. INTRODUCTION

The application of radar to meteorological observation was the critical development initiating the proliferation of convective storm analyses during the past twenty-five years. Early comprehensive studies, typified by Byers and Braham (1949) have been followed by numerous treatises dealing with various aspects of convective storms, with the emphasis on severe storms (i.e., those associated with damaging surface winds, large hail, and/or tornadoes). Most of these studies have been confined to a single storm case or a limited number of cases which displayed unusual or remarkable behavior and/or had come under scrutiny by one or more data gathering techniques including radar surveilance, surface mesonetworks, airplane reconnaissance (sometimes including chaff deployment), and balloon-borne soundings. Studies of this type, which have been primarily concerned with the airflow in and around storms and the motions of storms with respect to the environmental winds, have included those of Newton and Newton(1959), Browning and Ludlum (1962), Browning (1964), Newton and Fankhauser (1964), Charba and Sasaki (1968), Fujita and Grandoso (1968), Fankhauser (1971), and Marwitz (1972). As more and better data becomes available, many of the concepts and models previously developed are updated accordingly. Only since 1966, following the establishment of the rawinsonde mesonetwork of the National Severe Storms Laboratory in Oklahoma, has it been possible to study the mesoscale aspects of convective storm systems using large numbers of vertical soundings in conjunction with a

recording surface network and radar surveilance. This study addresses one such documented storm case in which the activity was intimately associated with an advancing cold front. This is in contrast to the majority of studies reported in the literature which tend to be concerned with air-mass storms or squall lines.

On May 14, 1970, a particularly long line of convective storms formed in association with a cold front moving southeastward through the central United States. A portion of this line passed through the 4000 km^2 mesonetwork of the National Severe Storms Laboratory, reaching its maximum development while in the network. A considerable amount of data was amassed during this event, including surface data from 44 automatic recording stations, vertical soundings from 58 rawinsonde ascents originating at nine launch sites, and continuous PPI radar coverage at elevations from zero to 20°. These storms developed under atmospheric conditions which did not display the extreme values of low-level moisture, instability, or middle-level winds characteristically associated with outbreaks of severe convection. (Whitehead, 1971). This data set does, nonetheless, provide an ideal opportunity for a detailed examination of a well-organized, extensive system of strong convective storms which was clearly frontal in its origin. Descriptions of the documented storm cases collected at NSSL from 1966 through 1970 (Barnes et. al., 1971) reveal few instances in which as many as 58 rawinsonde ascents accompanied a single case, particularly in conjunction with

a surface/ rawinsonde network as dense as the one existing in 1970. Thus, the quantity and quality of the data were major factors encouraging further examination of this case.

This study, which addresses both the qualitative and quantitative aspects of the available data, attempts to interrelate the surface, radar, and rawinsonde data to gain as complete a picture as possible of the mechanisms at work in this storm system. The system displayed two particularly interesting patterns of development during the period of observation. In the early stages the width of the radar echoes in the direction normal to the line axis was quite small and the net motion of the line toward the southeast frequently resulted from the formation of a separate and distinct line of new cells several kilometers ahead of the previous line position. One outstanding example of this occurred while the system was within the network and had an important effect on the distribution of rainfall. In the later stages, while the system was still within the network, the radar echoes increased markedly in width. These phenomena are addressed in some detail. The major result of this study derives from an analysis performed on the rawinsonde data which greatly increased its ability to describe the essential features of the overall storm system.

The sections which follow describe the mesonetwork, the synoptic-scale events associated with the storms, and the analyses performed on the mesoscale data. Assessments are made of the degree to which this storm system displayed the various characteristics generally attributed to severe convective storms.

2. THE 1970 NSSL MESONETWORK

The NSSL mesonetwork as it existed in 1970 included 44 automatic recording surface stations arranged in an approximately square configuration 35 nautical miles on a side and situated in central Oklahoma between about 35.1 N to 35.65 N and 97.4 W to 98.1 W (see Figures 1 and 2). The spacing of the stations in this β-network was somewhat irregular due to topographical and accessability factors but averaged about 5 nm. These stations ranged in elevation (msl) from 345 meters (8A) to 440 meters (W4) and each included a recording windvane and cup anemometer located on a mast 7 meters above the ground (NSSL Operations Staff, 1971). A microbarograph and a hygrothermograph were housed in an instrument shelter, and a recording rainguage was situated near ground level at a suitable distance from other objects. All data were recorded as continuous traces with the exception of wind direction. This was sampled at one-minute intervals, with any of the eight compass points which occurred during the minute being recorded. Rawinsonde launching and tracking facilities were located at nine of these sites, distributed through the network (Barnes et. al., 1971) and indicated by circles on Figure 1.

The 1970 network was a refinement of similar networks which had been operated in various configurations during April and May since 1966. Like the 1969 network, it covered a smaller area than those operated prior to 1969, but had more closely-spaced stations. Experience gained in previous years was used in determining the 1970 operational procedure for the

rawinsonde ascents. On operational days when convective activity was expected or was located outside the network, routine serial soundings were made to 250 mb on roughly an hourly basis. When storms were within or very near the network, soundings were generally made only to 400 mb to allow for a more rapid sequence of launches. An open schedule of launches was permitted at each site, with no attempt to coordinate with the activities of the other sites. Past experience had shown that attempting simultaneous releases or adhering to a fixed schedule was not desirable for maximizing sounding data.

Radar coverage was provided by a WSR-57 10 cm radar, located at the NSSL headquarters (station 5E) in the southeast portion of the network. This radar continuously sweeps in azimuth, generating three complete PPI displays per minute. The elevation angle is nominally zero, but an automatic sequence can be initiated at regular intervals in which the elevation angle is increased by either 1.0° or 2.0° on each sweep (depending on the range of the echoes) to a maximum elevation sufficient to include the highest echoes, but limited to 20°. Following the last (highest) elevated sweep, the elevation returns to zero until the next sequence begins. The display on each sweep consists of up to five intensity regimes in the effective radar reflectivity parameter, Z. On the odd-numbered frames the threshold values are defined by $\log Z = 1.0, 2.0, 3.0, 4.0, 5.0$, while on the even-numbered frames they are 5 dbZ higher.

3. SYNOPTIC-SCALE ASPECTS

Figures 3, 4 and 5 present, respectively, the surface, 850-mb, and 400-mb synoptic analyses over the south-central United States for 1800 CST May 14 (0000 Z May 15). The most noteworthy feature on the surface analysis is the trough extending from northern Indiana and Illinois southwestward into New Mexico. A strong front lying within this trough separated cool air to the north from warm, rather moist air to the south. This front was moving southeastward and at 1800 CST was just entering the NSSL mesonetwork. The surface wind flow in the southern plains was uniformly from the southeast off the Gulf of Mexico, veering to SSW in the near-frontal region. Numerous squall-line thunderstorms were occurring from Missouri to Indiana, and produced widespread one to three-inch rainfall amounts. Cloudiness associated with a large area of air-mass showers in central Texas had produced a general lowering of the temperature in this region, and several 24-hour rainfalls of over two inches were reported. The 850-mb wind field displayed the same character as that at the surface, indicating a broad, rather moist flow into the southern plains from a southeasterly direction. A tongue of warm air ahead of the frontal trough extended into central Oklahoma from the southwest.

The 400-mb analysis shows a deep short-wave trough in the upper Great Plains with a weaker extension into western Oklahoma and Texas. This suggests conditions mildly favorable for upward motion over Oklahoma. The

region of maximum winds lay well to the north of Oklahoma, with Oklahoma City reporting only a 15 knot wind from the southwest at 400 mb. Worthy of note is the strongly ageostrophic nature of the wind reported at Abilene, Texas, being 30 knots with a bearing of 160° in a region where a west wind at a lesser speed would be expected. It is possible that this wind represents an outflow from the large region of convective activity over central Texas.

Examination of the rawinsonde soundings taken on May 14 at the Oklahoma City station of the USWB reveals conditions favorable for the development of convective activity. Figures 6 and 7 present the temperature and dewpoint soundings taken at 0600 and 1800 CST, respectively. The morning sounding shows that the air below the 825-mb level was quite moist and the lapse rate was conditionally unstable at most levels above 880 mb. By 1800 CST, the moisture had decreased somewhat at levels below about 800 mb, while showing an increase above this level. The conditional instability existed at essentially all levels from the surface to 500 mb. The precipitable water represented by both of these soundings was about 0.95 inch (surface to 500 mb). Also indicated on Figures 6 and 7 are the winds at the standard pressure levels. Notably absent at both times was the strong wind shear with height normally associated with severe convective storms (Browning, 1964). The Lifted Index (LI) computed from these soundings and reported by NMC was -2 in both cases, a level which indicates

a good thunderstorm potential but which is not considered an extreme value (Galway, 1956).

A relatively new index of convective potential was developed in the late 1960's based on a study of 328 severe weather cases collected at the Military Weather Warning Center (Whitehead, 1971). Called the Severe Weather Threat (SWEAT) Index, it consists of three terms characterizing 1) the low-level moisture, 2) the static stability of the air mass, and 3) the environment winds. It is very easily calculated by hand using only the temperature and dew point at 850 mb, the temperature at 500 mb, and the wind speeds at 850 and 500 mb. A value of 250 is considered the threshold above which severe convective activity can develop, while 350 or higher indicates a potential for tornadic storms. The values of the SWEAT index computed from the 0600 and 1800 CST Oklahoma City soundings are 346 and 189, respectively, the decrease being primarily attributable to the decreases in the 850-mb values of dewpoint and wind speed. It is not unreasonable to believe that the morning value overstates the potential, as the 35-knot 850-mb wind is not typical of the lower troposphere on this sounding. Similarly, the large relative decrease noted in the afternoon value seems misleading, since the greatest decrease in moisture happened to occur at the 850-mb level used in the calculation. Taken together, the LI and the SWEAT index do seem to indicate a potential for convection of marginally severe character, at most.

Examination of hourly reports from a number of weather stations in Oklahoma (see Figure 2) shows that the cold front moved slowly through the northwestern portion of the state during the morning, passing Gage at around 0800 and producing no precipitation. The first visual reports of cumulonimbus development came from Vance AFB near Enid, which reported them to the north at 1400. The film record of the NSSL radar display commenced at 1407 CST, and at this time the only visible echoes were three weak cells indeed located 20 to 30 miles NNE of Enid. The front accelerated during the afternoon, passing Vance AFB at 1516 CST. Until about 1600 CST, the radar echoes were quite weak and short-lived with most of them scattered over a lightly populated region to the southwest of Enid. At about 1600 CST, a new cell formed about 20 miles SSW of Vance AFB and quickly developed into a large, strong storm which moved toward the E or ESE (to the right of the environment winds) and persisted for well over an hour. Vance AFB, on the northern fringe of the storm, received 0.04 inch of rain while Enid, less than ten miles to the ENE, received none. By 1700, numerous weak cells began to form a distinct storm line through the western half of the state and by 1800 the line extended beyond the area displayed on the radar scope, a distance of nearly 200 nm, with only a few small gaps and numerous fairly strong cells. At this time the leading edge of the line was less than 20 miles from the northwest corner of the network. The front passed through the

Oklahoma City area between 1900 and 2000 CST, passed Tulsa shortly after 2000 and reached Fort Sill at 2040. Thunderstorms occurred at all three of these locations, with Oklahoma City (USWB) reporting the largest amount of rain, 0.90 inch. Small hail was reported at Fort Sill and at Hobart, both located some 55 to 70 nm to the WSW of Norman, well outside the mesonetwork. No precipitation or evidence of frontal passage was reported through midnight from stations in the southeast corner of the state (McAlester, Ardmore).

The typical sequence of weather events reported at stations in central Oklahoma showed a cirrostratus overcast present essentially all day. Preceding the arrival of the cold front, Cb were typically observed in the northwest quadrant. Following cold front passage, a low overcast moved in accompanied by thunder and lightning to the west and north. Fifteen minutes to one hour later rain began, accompanied by frequent lightning, in-cloud and cloud-to-ground. Rainfall was generally reported as light to moderate and lasted for several hours, becoming quite light in the later stages. The lightning became less frequent and moved away toward the east after two to three hours. At Fort Sill, the thunderstorm activity began about one hour prior to the arrival of the cold front, and continued after its passage, Examination of the radar data shows that this was caused by an isolated air mass storm which merged with the main storm line.

4. MESOSCALE ASPECTS

As outlined above, the convective storm activity gradually increased in intensity and areal extent between 1400 and 1800 CST. Fortunately, one of the best developed portions of this activity moved through the NSSL mesonetwork during the time the storms were achieving their maximum development. All elements in the network performed well, generating a gratifying amount of data and thus presenting the opportunity for a detailed mesoanalysis of a system of convective storms of frontal origin.

The following sections discuss, in turn, the analyses conducted using the data from the surface stations, the films of the radar display, and the data from the rawinsonde ascents.

A. Analysis of Surface Data

Of the available recorded surface data from the 44 stations in the network, the quantities displaying the most character were the winds and the rainfall. Taken together, these parameters do much to reveal the basic character of the storm system. Prior to the arrival of the cold front at the surface, the wind at a typical station was blowing rather steadily from a direction between SSW and SE with a speed of about 10 knots and with minimal gusting. In the few minutes preceding the arrival of the front, the wind speed gradually decreased to about 5 or 6 knots. The passage of the front was marked by a rapid increase in wind

speed to about 15 or 20 knots with an attendant veering of the wind to a direction between NW and NE. This veering of about 180° was generally accomplished in one to three minutes, after which time the wind displayed moderate gustiness and a tendency for the direction to switch between NNW and NNE at intervals of tens of minutes. Often these changes in direction were accompanied by perceptable changes in the average wind speed.

No precipitation was observed in the immediate vicinity of the surface front and, in general, rainfall did not commence until 40 to 70 minutes after the passage of the front. The precipitation, once it did begin, was widespread, with every reporting station experiencing measurable rainfall within 90 minutes after frontal passage.

An overall qualitative examination of the surface data traces clearly indicates that the wind shift phenomenon was associated with a true cold front and was not a mesoscale feature resulting from downdraft-produced gust fronts or a squall line. Once the wind shift was accomplished at each station, there was not a single instance of subsequent departure of the wind from directions with northerly components. Temperatures fell steadily from their prefrontal values in the low eighties into the upper fifties without ever showing any recovery. In short, no evidence of a squall line separate from the front could be found, and this outbreak of convection must be considered strictly frontal in nature. The traces of barometric pressure,

temperature, and humidity were uniformly unremarkable and were not quantitatively studied in this analysis.

1. Wind

Close examination of the wind traces reveals a markedly uniform progression of the wind shift phenomenon through the network. The time of wind shift at each station has been defined as that time at which the recorded trace first shows a wind having a northerly component. Figure 8 gives the time history of the progression of this wind shift through the network, from its first appearance at station R5 at 1754 CST until it passed the last station, R1, at 2029 CST. The instantaneous locus of the wind shift will hereafter be designated the surface wind shift (SWS) line. The progression of the SWS line through the network was at a somewhat greater speed in the earlier stages than it was later on. Presented in Figure 9 is the distribution of maximum wind gusts reported in the network. The greatest value was 44 knots at station W2, with only two other stations reporting as high as 40 knots. The high values reported in the southwestern part of the network correlate well with the region of heaviest rainfall (see following section) and apparently occurred when the system was at its maximum strength. The 25-knot isotach roughly encloses the Oklahoma City metropolitan area and appears to demonstrate a wind speed reduction due to urban structures. The 36-knot gust at station WRN (see Figure 1 for stations) occurred near the right flank of a strong storm cell. This station is in a very flat, exposed location. Based on

these reported wind gusts, it could be concluded that the storms were of moderate intensity at most. However, a layer of cold stable air about one km deep existed beneath these storms (discussed in Section 4.C) and may well have prevented stronger winds from reaching to ground level.

ii. Rainfall

The distribution of rainfall amounts that occurred at each station during the three-hour period following the passage of the SWS line is presented in Figure 10. This time period was selected to include the effects of the principal storm line, while excluding the rainfall associated with a widespread area of lighter rain which moved through part of the network after 2200 CST (see Section 4.B below). The isopleths on this figure were drawn using the radar data as a guide. Immediately apparent is the widely scattered character of the heavier rainfall amounts in the northern portion of the network as contrasted to the large region of rather uniformly heavy amounts in the southern portion. A distinct band in which practically no rain fell lies across the northwestern part of the network. The storm system behavior responsible for the main features of this rainfall distribution are discussed in detail in the radar data analyses of Section 4.B. Although several stations in the southern part of the network reported about two inches of rain, this can be attributed fully as much to the broad, slow-moving character of the system in this region as it can to the intensity of the rain cells.

B. Analysis of Radar Data

The mode of operation of the WSR-57 radar has been discussed in Section 2. On May 14, 1970, the film record of the PPI display commenced at 1407 CST and provided a continuous record of 1645 frames through 2330 CST. The elevated scan sequences, initiated every five minutes, began at 1530 and were terminated after 2120. The most apparent feature of the storm system revealed by the radar data is the nearly unbroken linear arrangement of the cells at any given time. Once the line became well organized, it extended for 300-400 miles (Barnes et. al., 1971) with very few gaps. In the vicinity of the NSSL mesonetwork, the line of strongest echoes was always closely parallel to the SWS line, but with its leading edge lagging the SWS line by about 15 nm. Qualitative examination of the radar data revealed three distinct phases in the precipitation pattern observed within the network.

1) In the early stages, the line of radar echoes was only 3 to 10 miles in width, the individual cells were easily distinguished and arranged in a strikingly linear pattern, and the areas receiving the heaviest precipitation were relatively small and widely scattered. Figure 11 shows the zero elevation echo pattern at 1900 CST, and is representative of this early phase.

2) Between 1930 and 2030 the width of the line underwent a considerable increase, so that in its later stages the echoes were about 20 miles wide and showed a widespread

region of rather heavy precipitation with the individual cells less sharply defined but more numerous. The zero-elevation echo pattern at 2100 is depicted in Figure 12. In the area immediately southwest of the network, the echo line was nearly 40 miles wide. Individual cells were much more numerous and more randomly positioned than they were at 1900. The most intense cells were located in the region obscured by ground clutter. Subsequent to this time, the intensity of the cells comprising the storm line began to show a decrease. The region of heaviest precipitation, greatly reduced in size, had passed beyond the network by 2230.

3) Between 2200 and 2400 a large area of widespread light rain moved from WSW to ENE across most of the network. This precipitation, situated far beyond the cold front, is of uncertain origin. It may have been associated with the sheared off remnants of storms occurring to the southwest of the network. It is of no further interest in this study.

Shown on Figure 13 are the tracks followed by the majority of the identifiable individual storm cells visible on the radar display between 1730 and 2220 CST. The centroid of the most intense part of each cell as it appeared at zero elevation has been plotted at ten-minute intervals. All cells that were identifiable at three consecutive ten-minute times are plotted. Numerals identify the positions occurring on the hour (i.e., 19 ≡ 1900 CST). Tracks not existing at any

whole hour have a half-past time identification indicated (193 ≡ 1930 CST). The last position on each track is indicated by an arrowhead to clearly establish the direction of motion. No information is plotted inside a range of about 18 nm due to interference from ground clutter. The locus of the strongest cells defining the storm line is indicated at half-hour intervals by broken lines. Unlike the SWS line, the storm line progressed southeastward at an irregular speed. Examination of these cell tracks shows the component of motion of the individual cells in the direction of effective storm line movement to be generally small but not zero. The line displayed its fastest net advancement due to the formation of new cells ahead of the existing storm line. As the newly-formed cells increased in strength, the older ones had a tendency to weaken and die out, thus producing a discontinuous advancement of the storm line. Figure 13 clearly shows this happening between 1800 and 1830 and again between 1900 and 1930. It is interesting to note that there is not a single instance of intersection of cell paths among those cells associated with the main storm line. Apparently the region favorable for cell formation, namely the large-scale saturation produced by frontal lifting, was a very limited region that was moving southeastward with the overall system, and once the local supply of saturated air was exhausted, no more became available in a given area. (It should be noted that the cell centered near azimuth 295°, range 50 nm at 2200 CST was not associated with the main storm line, but was in fact the

strongest of the echoes associated with the widespread area of light precipitation described in paragraph 3 above.) The hodographs inset on Figure 13 show the ambient winds at about 1800 CST and 2100 CST. The first (A) is taken from the official USWB rawinsonde ascent made at 1800 CST from Oklahoma City (near network station R6), while the second (B) was taken from a rawinsonde initiated at station R7 at 2053 CST. Both soundings indicate rather unremarkable amounts of wind shear with height in the warm air mass below 400 mb. The speeds at 1800 were quite low, but the wind did veer with height up to 500 mb. By 2100 the wind had increased markedly in speed up to at least 400 mb and had backed sharply at all levels except 850 mb, which was within the advancing wedge of cold air. Examination of the cell tracks shows that movement in essentially all cases was somewhat to the right of the environment winds at all levels in the warm air, a characteristic which Browning (1964) attributed to large and intense cells, and which is accomplished through continuous (as opposed to discrete) development along the right flank of the cell, a region in which a favorable nonhydrostatic vertical pressure gradient exists. In a strongly veering and sheared wind regime, a pressure deficiency aloft develops on the right flank due to increased speed of the environment winds, which are forced to flow around the slower-moving storm core (Newton and Newton, 1959). This pressure deficiency overlies the region of low-level convergence and its associated pressure excess, thus providing vertical acceleration for the

moist inflowing air and making the right flank a favored location for new cell development. These mechanisms appear to be present in this case and, though not impressive by classic severe storm standards, probably account for the observed rightward motion, particularly in the earlier stages (prior to 2000 CST) when individual cells were stronger and longer-lived. No examples of left-moving or splitting storms could be found such as those described by Fujita and Grandoso (1968) or Charba and Sasaki (1968). At least four of the cell tracks shown at the extreme bottom of Figure 13 have strong northward components to their motion; however, if we assume hodograph B describes the ambient winds, these too were right-moving cells (with respect to the winds in the warm air). At least two of these cells (labeled A and B) had their origin south of the advancing cold front. Perhaps more favorable atmospheric conditions, combined with slight orographic lifting as the low-level flow approached the Wichita Mountains (Figure 2), allowed these cells to develop in the absence of frontal lifting. Cell A produced rain at Fort Sill, Oklahoma, prior to the arrival of the SWS line (see Section 3). Both storms moved generally northward under the influence of the southerly winds at all levels, riding over the advancing cold air and eventually merging with the main storm line. In Figure 12, cell B appears at azimuth 225°, range 38 nm where it has just begun to interact with the main storm line.

As mentioned above, the storm line displayed its fastest net advancement due to the formation of new cells ahead of

the existing storm line. When the mature cells in the storm line were larger, quite strong, and relatively long-lived, as was frequently observed in the early stages of the system, regenerating cells often formed as separate entities some 5 to 10 nm ahead of the storm line, with the result that a distinct, precipitation-free region existed between the old and new storm line positions. The most dramatic instance of this occurred in the northern portion of the NSSL network, commencing at about 1900. Figure 14 is a rendition of the PPI display at 1910, elevation 4°. Three or four new cells are seen forming about 10 nm ahead of the strongest part of the line of older cells and 5 to 10 nm behind the SWS line. The line indicated by the arrows passes through the most intense portions of one of the old cells (A) and one of the new cells (B), selected for detailed examination because of their spatial proximity and because cell A was one of the strongest cells prior to the redevelopment, while cell B was the strongest afterward. Figure 15 shows the appearance of the PPI display at 1930, elevation 2° . The new cells have merged into a line of very strong echoes, while the older ones have weakened considerably. It is interesting to note the appearance of three new cells (labeled C,D,E) developing on the leading edge of the storm line. Cells A and B have moved eastward about 3 and 5 nm, respectively. Presented in Figure 16 are vertical cross-sections taken along the line connecting the most intense portions of cells A and B. These appear at five minute intervals from 1900 through

1940, and show cell B from the first appearance of echo-producing droplets through its development into a strong, mature storm. The first echo noted in cell B appeared at about 1900 near the 7-km level and reached the ground at 1910. By 1915 the cell was producing heavy precipitation over a small area at the surface. The first appearance of an anvil-like formation on this cell is noted at 1930. The track of this cell was in the vicinity of station 3C, which received 1.40 inches of rain. At 1940 some propagation of the storm along its right flank is noted. Subsequent to this time, cell B weakened as new activity formed to the southeast, too close to the radar site for worthwhile examination. At 1900 storm A appears to be near its maximum development with a core of moderate to heavy rain and a well-defined anvil. The appearance of cell B apparently marks the cessation of the updrafts feeding storm A, for the precipitation gradually falls from it, until at 1940 only an anvil-like structure remains. The various contributions to the apparent motion of the storm line may be determined directly from Figure 16, since the plane of these cross-sections is very nearly perpendicular to the storm line. During the 40 minute period, the center of most intense rainfall advanced 12 nm, while cell B advanced only 1 or 2 nm. By far, the major contribution to the net motion is the formation of cell B, which is centered 11 nm ahead of A at 1900 and 7 nm ahead at 1940. Although the net effect of this phenomenon was to move the center of most intense rainfall from a range of 30 nm to a range of 18 nm,

the most interesting fact is that during this process, no rain whatsoever occurred between ranges of 22 and 24 nmi.

Although Figure 16 illustrates the dramatic growth of a single cell, this event is even more striking when viewed along its entire 40 nm length. Figure 17 is a cross-section down the lengths of the old and the developing storm lines at 1910 and 1920, plotted on a height-azimuth angle plane as viewed from the radar site. The cross-sections are somewhat idealized, passing through the maximum intensity portion of each individual cell. The numerical scales in Figure 17 were selected to approximate a one-to-one correspondence between vertical and horizontal length dimensions. Cells A and B from the previous discussion are indicated on the figure. At 1910 the portion of the main storm line depicted has six mature cells and one growing cell, while the developing line has nine identifiable cells in various stages of growth with at least four of these beginning to produce precipitation at the ground. At 1920, all of the mature cells in the old storm line have weakened appreciably, while the developing cells have taken over as the main storm line. At least four new cells are producing heavy precipitation at the ground, and at least six other new cells in various stages of development are detectable.

The lateral extent of this new line generation was such that it spanned essentially the entire width of the mesonetwork from east to west. The effects of this development on the distribution of precipitation are clearly revealed by

Figure 10. The 1.54 inches at station R5 and the 0.53 inches at W7 were produced by cell A or its near neighbors. The 1.5 inch maximum near station 3C was produced by cell B in its late stages. Lying between these maxima is a broad region in which the amounts were under 0.1 inch. This region of near-zero precipitation was produced in exactly the manner described above in conjunction with Figure 16.

In the later stages of the storm line evolution, when the echoes were broad and comprised of widespread, rather indistinct cells, the advancement was characterized by the appearance and development of new cells along the leading edge of the storm line. As these cells grew, they quickly merged with the main echo band, whose rear flank typically showed a gradual weakening. (See Figure 12 for representative examples of this renewal and weakening.)

Attempts were made to determine the mechanisms responsible for initiating the redeveloping storm line. The rawinsonde data described below, while providing impressive coverage by most standards, was too widely spaced and infrequent to provide an adequate description of the three-dimensional distribution of the important meteorological variables associated with these brief events. These aspects are examined more fully in Section 4.C. There was, however, interesting behavior associated with the surface winds at the time the new storm line was developing. The speed and direction of the flow at the surface in the vicinity of the storms was most strongly controlled by the low-level cold air advection

behind the surface front. The convective activity was actually occurring in the warm air mass under which the cold air was driving, so the surface wind field did not display the dramatic regions of inflow and outflow often observed in air-mass or squall line storms (NSSL Operations Staff, 1971). The surface wind field did display organized regions of divergence and convergence superimposed on the basic northerly flow and typically occurring on a scale greater than the spacing of the stations. These produced the periodic fluctuations of wind direction and speed mentioned earlier. Figures 18 through 22 show the essential features of the surface wind field divergence and its relationship to the radar echoes at ten minute intervals from 1850 to 1930. The divergence field was determined by calculating, at the appropriate time, the x and y components of the surface wind. The distributions of u and v so determined were mapped onto a rectangular grid from which fields of $\frac{\partial u}{\partial x}$ and $\frac{\partial v}{\partial y}$ were determined. These fields were graphically added to obtain the divergence field, $\frac{\partial u}{\partial x}+\frac{\partial v}{\partial y}$. In general, one would expect to find the regions of strong convergence upwind in the low-level feeding flow (i.e., toward the south or southeast) from developing or mature echoes, and the strongest divergence beneath strong echoes or decaying cells. Figure 18 shows that at 1850 the wind field had little character. A region of modest divergence is noted beneath what appears to be a small developing cell on the leading edge of the main storm line. This would tend to indicate that the small cell was not really developing. At 1900

(Figure 19) the main storm line was beginning to decay slightly with modest divergence in evidence. Little additional development occurred in the small cell north of station 4A. Regions of convergence were appearing, with the strongest located directly beneath a group of small developing echoes. At 1910 (Figure 20) the divergence beneath the old cells had increased, a reflection of precipitation-induced downdrafts. Two main areas of convergence were associated with the line of growing cells. A similar situation existed at 1920 (Figure 21) with the new cells forming a strong line and the old cells decaying rapidly. By 1930 (Figure 22) the convergence associated with the new line had subsided, indicating that many of the cells in the line had probably reached their maximum development. One of these cells, centered near station 4A, was in fact weakening and producing a strong divergence. New cells were appearing along the forward flank of this cell.

In summary, although the divergence of the surface wind field appears to correlate well with the character of the radar echoes existing at the same time, there does not seem to be, within the accuracy of this analysis, any causal relationship explaining why the new cells formed where and when they did. If this cell formation were related to perturbations in the height of the cold/warm interface caused by outflowing cold air from the main storms, then features of the wind field should lead new cell development by at least a few minutes and there is no evidence of this. The triggering mechanism must be a property of the warm air feeding the main storm line and

is addressed in the discussion of the rawinsonde data which follows.

C. Analysis of Rawinsonde Data

During the afternoon and evening of May 14, 1970, a total of 58 rawinsonde ascents were made from the nine sites within the NSSL mesonetwork. The first of these was released from station R3 at 1530 CST and the last at 2210 from station R5. Of the 58 soundings, 26 were released prior to the arrival of the SWS line at the launch site and 32 were released afterwards. Figure 23 summarizes the ascents at each site, indicating time of release and the time and pressure level of the last received data. Five of the balloons, indicated by asterisks, descended back to ground level after reaching various heights. The reasons for these descents are unknown, but could include leaks and icing. In general, much of the transmitted data during descent appeared to be of questionable validity. Figure 23 shows that the frequency of release was very good at most of the stations.

The following section discusses the redeveloping storm line with reference to the appropriate individual soundings and offers an explanation for its occurrance. The interesting behavior of the 400-mb wind field as revealed by the individual soundings is examined in the subsequent section. Finally, an analysis of the rawinsonde data is presented in which the soundings were statistically combined in a way that allowed examination of the major characteristics of the storm system.

1. The Redeveloping Storm Line

Although the radar and rainfall data clearly showed the dramatic generation of a new cell line in the northern part of the network between 1900 and 1930, they have contributed little toward explaining the mechanisms responsible for such an event. The character of the surface wind field has shown it to be unlikely that the new cells form in response to downdraft-induced perturbations to the lifting along the advancing cold front. Examination of the individual rawinsonde ascents was made to identify those which occurred in the vicinity of this event and to select others to be used as controls for comparison. Accepted for this latter group were all which occurred near the leading edge of the echoes or within ten miles to the southeast and were in a region of adequate radar coverage. The entire sample so determined consists of only seven soundings, three of which occurred in the vicinity of the redevelopment. Table 1 is a comparison of selected data from these soundings and includes wind, relative humidity and temperature. The temperature is characterized by the wet-bulb potential temperature, θ_w , selected because it removes the effect of height on the numerical value of temperature and because it is conserved for either moist or dry adiabatic processes. Only the first three of these soundings occurred in the vicinity of the redeveloping cell line. The others were taken at later times in the southern portion of the network, when new cells were tending to form along the leading edge of the storm line. The R5/1846 sounding was

made into the leading edge of a large, fairly strong echo just prior to the time when the new line appeared to the southeast. The relatively low values of θ_w make it seem likely that this is a region of mild downdraft and the light horizontal wind velocities are probably a manifestation of the tendency for large storms to act as barriers to the ambient winds (Fankhouser, 1971; Newton and Newton, 1959). The 5A/1852 sounding came very near the newly-forming cell line just prior to the time when its precipitation first reached the ground. It skirted the rear flank of one of the strongest new echoes and was about 5 miles to the southeast of the old storm line. The most interesting feature of this sounding is the high wind speeds at all levels above 850 mb. The R6/1916 sounding was made at about the time the newly-formed line of echoes was becoming quite strong. Although located outside the visible echo, this sounding was in a region of saturation and high θ_w, probably associated with the updraft feeding the new cells. Also indicated in Table 1 are the pressure levels at which the soundings passed into the layer of southerly winds. Comparison of the 5A/1852 value with the others gives no indication that a region of higher-than-nominal frontal surface is triggering the cells through enhanced lifting.

This limited sample of rawinsonde data is not adequate to provide an explanation of the mechanism of storm line redevelopment. The most reasonable premise is based on the qualitative observation that the dramatic instances of cell line redevelopment occurred when the cells in the old storm line

were large, long-lived and relatively strong. The following model is proposed to account for the formation of new cells, both along the leading edge of the storm line and in instances of storm line redevelopment.

1. The existing cells in the storm line travel somewhat to the right of the environmental winds due to continuous growth along their right flanks.
2. The component of this cell motion toward the direction of cold front advancement is considerably slower than the motion of the front.
3. The development of new cells is suppressed in the vicinity of existing cells due to moisture budget requirements. The larger and stronger the existing cell, the larger its region of influence.
4. As the cold front moves southeastward, the lifted region of large-scale saturation favorable for new convection follows it, eventually passing beyond the influence of existing cells.
5. New cells will develop in this saturated air if sufficient low-level moisture is available in the region. If the existing cells in the storm line are not strong and/or are only a few minutes old, then the new cells will be forming near them. If the existing cells are strong and long-lived, then the region of potential cell formation will have travelled a considerable distance to escape their influence and the new cells will appear as wholly separate entities.

ii. The Wind Field at 400 mb

Examination of the radar data has revealed that in the later stages (after 1930 CST), the storm line became wider and moved somewhat more slowly. The causes for these events become more apparent through examination of the soundings taken at each of the nine sites. In every case, the winds up to at least 400 mb and down to essentially the interface with the advancing cold air are observed to back sharply from WSW to SSE and to increase in velocity. An indication of this was given previously by the wind hodographs presented with Figure 13. A more detailed examination of this phenomenon has been conducted at the 400-mb level.

Presented in Figure 24 is the time series of wind observations at 400 mb for each station for the 52 soundings that actually reached this level. These are plotted at the actual times that the 400 mb level was passed. The speeds are indicated in knots and the wind direction to the nearest degree is tabulated. The triangles indicate the time of SWS line passage at the launch site. Until nearly 1900 CST the wind directions are quite uniformly between 240° and 250°. From about 1900 to about 2100, the winds generally back to directions between 160° and 190°, where they remain through the end of the data set. Figure 25 indicates that the backing of the wind was related in some measure to the frontal system. To construct this figure, each 400-mb wind direction was plotted as a function both of time and of the distance the balloon was from a reference axis parallel to the mean SWS line and arbitrarily

selected as passing through station 5A. As discussed in Part iii below, the mean SWS line was determined to lie 55° to the right of true north. In this coordinate system, features whose principal movement with time is from northwest to southeast will appear as downward-sloping lines. The passage of the SWS line and the onset of precipitation are indicated on the figure and their southeastward movements are apparent. Isogons of the 400-mb wind field are indicated on the figure at 10 knot intervals. The marked uniformity of the wind direction prior to the onset of the backing is clearly illustrated. Little or no backing occurred at any station prior to the arrival of the SWS line, but after its passage, a backing of 30 to 40 degrees quickly followed at all but R4 and R5, the most northwesterly stations. Here, the backing was delayed for about an hour. With the exception of these two stations, the backing to about 210° appears to move southeastward at about the same speed as the front. The remaining backing tends to appear first near the middle of the network and to spread both ways from there. This backing of the wind clearly was ageostrophic, otherwise observed temperatures in the southwest part of the network would have been notably lower than those to the northeast, a phenomenon which did not occur. It is reasonable to believe that frotogenesis was occurring in this region at this time. Examination of the 1800 CST 850-mb synoptic analysis (Figure 4) indicates a horizontal deformation wind field of a type classically associated with frontogenesis (Petterssen, 1956). This feature is present in the surface analysis as well (Figure 3),

but to a lesser degree. This type of wind-temperature interaction produces an intensification of temperature contrasts and an increase in relative vorticity. When the relative vorticity is no longer small compared to the Coriolis parameter, the ageostrophic circulation becomes important, producing the tilt of the front and the upgliding motion over this slope. Hoskins and Bretherton (1972) have examined frontogenesis using numerical models, showing, among their conclusions, that latent heat release enhances the process. The backing of the winds observed in the 14 May 1970 case must be caused by an intensifying ageostrophic circulation produced by a strengthening of the front and enhanced by the latent heat release in the storms. Hoskins and Bretherton caution that extensive Cb development might cause their models to be of little relevance, but in this case the storms seem to definitely have had an intensifying effect on the frontal ageostrophic winds. One sounding, taken at station R5, in the extreme northwestern part of the network after 2200 CST (see Figure 25) seems to indicate that the wind is beginning to recover some of its earlier character. At this time, the radar data indicated that the activity in the main storm line was becoming much weaker. Figure 26 presents the 400-mb synoptic analysis at 0600 CST, May 15 (twelve hours after Figure 5). There is no indication of an ageostrophic wind at Oklahoma City or at any other station, and, in fact, the Oklahoma City wind has veered somewhat from its 1800 CST, May 14 value. (The ageostrophic wind noted at Abilene, Texas, on Figure 5 had also all but disappeared by 0600.) Examination

of the 850-mb analysis for 0600 (not shown) reveals that the temperature gradient across the front had weakened from its appearance twelve hours earlier. Therefore, if frontogensis was responsible for the observed wind anomaly, the process must have reversed between 2200 and 0600.

Near the time of SWS line passage, the 400-mb winds at the three southernmost stations (CHK, R7, R1) display an anomalous brief veering of 30 to 40 degrees. The radar data shows no precipitation echoes in the vicinity, and the soundings show no saturated regions at any lower levels. The phenomenon disappears below about 500 mb on all three of these soundings and it appears on no others. Its cause is unclear, but must be a kinematic response to the lifting caused by the advancing front.

iii. A Technique for Combining the Rawinsonde Data

The large number of soundings taken during the passage of this storm system makes possible a good definition of the first-order distribution of meteorological variables within the system. It is necessary, however, to make some judicious simplifying assumptions to in effect "filter out" the smaller scale phenomena and thus maximize the usefulness of the soundings. Data presentation problems notwithstanding, even with 58 ascents the data is far too sparse to permit including variations in all three spatial dimensions and with time. The organization of the system into a well-defined line facilitates the simplification process by permitting the assumption that variations along the line axis are not of interest and are, in the

mean, zero. Figure 27 is a sketch showing the coordinate system which has been defined to facilitate processing of the raw-insonde data. The x-axis is aligned with the mean SWS line and is assumed to point 55° to the right of true north (based on the mean orientation of the SWS line as depicted in Figure 8). The positive y-axis then points toward the rear of the storm system, while the positive z-axis extends upward from the ground plane. The origin of this coordinate system is assumed to always lie on the mean SWS line and to move with it at a velocity given by

$$V_{sws} = -0.4\ \hat{\jmath}\ (\text{km min}^{-1})$$

where $\hat{\jmath}$ is the unit vector in the y-direction. A time coordinate axis, t, may be defined coincident with the y-axis, positive t-values giving the time since the SWS line passed the point presently located at y:

$$t = y/V_{sws}.$$

The most significant meteorological variations are those in the z and y directions. A convenient way of analyzing these variations is to plot each balloon sounding in the z-t plane, ignoring the x-coordinate in all cases. At a given altitude, the t-coordinate of balloon is conveniently determined from

$$t = T_o - T_{sws} + \Delta T - R \sin (\phi - 55^o)/V_{sws}$$

where

T_o = time of balloon release

T_{sws} = time SWS line passed release station

ΔT = elapsed time since balloon release

R = ground range from balloon to release station

ϕ = azimuth of balloon from release station

and the latter three quantities are read directly from the listings of the sounding data. If the storm system were indeed uniform in the x-direction and not changing its y-z configuration with time, then each of the 58 soundings could be taken at face value. The previous examination of the radar data showed that these uniformities certainly do not exist, so the adjacently plotted soundings from different stations display considerable irregularity. These irregularities are smoothed by grouping adjacent (in t) soundings and assuming that the averages of the meteorological variables within the group define a single sounding. It is hoped that the z-t distributions of the variables so obtained will preserve the essential character of the storm system, averaging out the effects of the growth of the system while masking the effects of small scale and short term anomalous behavior.

From the available soundings, 40 were selected for use in this analysis. This group includes all soundings initiated at t>-60 min., with the exception of those which descended back to ground level (see discussion under 4.C.). These 40 soundings were then grouped into seven overlapping sets of ten soundings each.

iv. Distribution of Significant Meteorological Variables

Temperature

The temperature distribution in the system has been characterized by the wet-bulb potential temperature, θ_w, selected to include the effects of moisture while eliminating

the effects of height on the numerical values of temperature. It is a quantity whose value is conserved for either moist or dry adiabatic processes. An increase of θ_w with increasing height usually indicates a stable lapse rate, while a decrease with height is associated with a lapse rate that is at least conditionally unstable. Presented in Figure 28 is the distribution of θ_w in the z-t plane, obtained by evaluating the seven sounding groups at ground level and at heights (msl) of .6, 1.2, 1.8, 2.4, 3.6, 4.8, 6.0 and 7.2 km. Also indicated (broken lines) is σ_θ, the root-mean-square deviation of θ_w, a measure of the non-uniformity of the grouped soundings. This would tend to be highest in those regions of the system where substantial x-variations or changes with time existed. Prior to the arrival of the SWS line, the distribution of θ_w shows the air mass to be unstable up to about 5 km, in agreement with the 1800 CST OKC sounding shown previously in Figure 7. The values of σ_θ are low in this region, indicative of the uniformity of this air mass. The arrival of the SWS line bodily lifts the warm air, and shortly afterward a region of high σ_θ appears, centered at about t=30 min and z=6 km. It is likely that this high σ_θ is associated with the scattered development of new convective cells, with some of the soundings passing within these cells and others not. Support is given for this notion by reexamining Figure 16. At 1905 the SWS line is located at a range of 11 nm. The developing cell B is centered at about 19.5 nm and height 5-7 km. Converting the range difference to a t-coordinate gives t = 21 min. This developing cell is

indeed centered in the region of maximum σ_θ. In examining Figure 28 and succeeding figures, it is helpful to note that the selected scales produce a vertical exaggeration of 8 to 1. Toward the rear of the system a lesser maximum in σ_θ of unknown cause is noted at low levels. In the region beyond t = 160 min., θ_w displays an average neutral stability below 4 km and is stable above this level. The net effect of the system has been to redistribute θ_w into a more stable configuration. The high θ_w (>20° C) air has apparently been transported to high levels (>6 km) in the convective cells. Convective mixing and entrainment with some of the low θ_w air at middle levels has caused the post-storm maximum values to be only about 18.5°C. The remainder of the low θ_w air (<16°C) must have descended in downdrafts to mix with the advecting low level cold air behind the front (θ_w <17 C).

Relative Humidity

The distribution of relative humidity in the system appears in Figure 29. Prior to the arrival of the SWS line, the humidity is moderate at lower levels and quite low at higher altitudes. The arrival of the SWS line creates a region of large-scale saturation, which appears in the averaged data as a region of RH>90% lying between 1 and 4 km. This is produced by the bodily lifting of the warm air mass by the thrust of advancing cold air. The size and numbers of convective cells which can be produced from such a region is limited; hence, as was the case for σ_θ, the scattered developing cells produce a region of high σ_{RH} centered near t = 30 min and z = 6 km.

A lesser maximum in σ_{RH} is noted toward the rear of the system, but not in the same location as the secondary σ_θ maximum. These are likely results of some minor feature in the system which was not traveling at the same speed as the SWS line. The tongue of high RH (>80%) extending leftward is probably a reflection of the anvil cloud. The region of high (>90%) low-level RH in the rear of the system is probably produced by the lowering temperature of air made moist by falling rain. This RH maximum corresponds closely in shape and location to a minimum in the θ_w field (see Figure 28).

Horizontal Winds

Figures 30 and 31 present, respectively, the distributions of u and v, the x- and y-components of the wind field relative to the ground as determined from the soundings. Positive values of u indicate motion into the page, while positive values of v indicate motion toward the rear of the system. The u-distribution displays southwesterly components in the warm air, northeasterly in the cold. Of interest is the zone of maximum speed lying just ahead of and above the regions where high σ_θ and σ_{RH} were noted. The flanks of strong storms are known to be favored regions for speed maxima in the mid-tropospheric winds (Newton and Newton, 1959; Fankhauser, 1971), and this maximum in u is indeed located on the right flank of the region of developing cells. The v-distribution shows a strong flow at middle levels behind the SWS line, a kinematic response to lifting produced by the advancing front. The average observed speed of the SWS line is about -7m sec^{-1},

close to the low-level average value of v, and it is apparent that the low-level flow itself is the mechanism producing the motion of the SWS line. It is reasonable to assume that the u = 0 and v = 0 contours approximately define the cold frontal surface at the lower values of t.

Vertical Wind

If the horizontal variations in density are neglected, the vertical velocity, w, is related to the horizontal wind field by

$$\rho(z)\left[\frac{\partial u}{\partial x} + \frac{\partial v}{\partial y}\right] = -\frac{\partial}{\partial z}(\rho w). \qquad (1)$$

A straightforward graphical solution of the vertical velocity distribution is possible if it is assumed that the divergence of the x-component of the wind field is negligible:

$$\frac{\partial u}{\partial x} \ll \frac{\partial v}{\partial y}.$$

This is a justifiable assumption in this line storm case and allows simplification of (1) to

$$\rho(z)\frac{\partial v}{\partial y} = -\frac{\partial}{\partial z}(\rho w).$$

The value of ρw at a given height is found by integrating upward from the ground (z_G):

$$\rho w(z) = -\int_{z_G}^{z} \rho \frac{\partial v}{\partial y}\, dz$$

subject to the boundary condition

$$\rho w(z_G) = 0.$$

The distribution of ρw so determined appears in Figure 32. It shows the air in the prefrontal region to be subsiding at altitudes above 2 km. The arrival of the SWS line with its underrunning cold air imparts a sudden upward motion at low levels. As this lifted air saturates and becomes unstable, it

feeds a large region of strong updraft, centered near t = 90 min in this averaged storm system. The convective activity destroys the instability, and in the region beyond t = 140 min there is little vertical motion at any height.

Stream Function

It is possible to combine the v and w information to define a stream function, ψ, which depicts the overall motion of the air in the z-t plane. The stream function is defined by

$$\frac{\partial \psi}{\partial z} = \rho v$$

$$-\frac{\partial \psi}{\partial y} = \rho w$$

or equivalently,

$$\psi(z,y_i) = \int_{z_o}^{z} \rho v dz + \psi(z_o,y_i), \qquad i=1,..,M \qquad (2)$$

$$\psi(y,z_j) = -\int_{y_o}^{y} \rho w dy + \psi(y_o,z_j), \qquad j=1,..,N \qquad (3)$$

If z_o is taken to be the ground, where $\rho w = 0$, then $\psi(y,z_G) = \psi(y_o,z_G)$, and the distribution of ψ may be determined using (2) alone, by integrating ρv in the vertical at several y locations. Since it is not desired to assign specific values to ψ, but rather to determine the shape of constant-ψ lines, $\psi(z_o,y_i)$ may be arbitrarily selected as zero. In order that the ψ contours approximate the actual average trajectories of air parcels, the value of v used in (2) must be relative to the SWS line:

$$v_{rel} = v + V_{sws}.$$

Figure 33 depicts the streamlines determined in this manner. The spacing between adjacent lines was arbitrarily selected to be 8000 kg m^{-1} sec^{-1} to produce an attractive display. The average speed of the mass flow between any two streamlines is

inversely proportional to the spacing between them. Since the motion of the cold air behind the frontal surface is nearly the same as the SWS line itself, a very low average speed appears in this region (no streamlines). The initial upward motion imparted to the warm air at the SWS line is apparent, as is the further increase in upward motion resulting from the unstable saturated air. The strong flow at high levels which shears the anvils and carries precipitation beyond the updraft region is also clearly indicated.

Water Budget

An assessment was made of the partitioning of the water vapor and condensate within the system using the calculated distributions of θ_w, RH, v, and ρw along with the traces from the surface recording rainguages. These latter traces were used to define the t-variation of the average measured rainfall rate, $\bar{R}_m(t)$. The trace for each station was divided into ten-minute intervals beginning at the time of the SWS. Then

$$\bar{R}_i = \frac{1}{42} \cdot \sum_{j=1}^{42} \frac{(r_{i+1}-r_i)_j}{10 \text{ min}}$$

where

r_i = the total rainfall up to time t_i

r_{i+1} = the total rainfall up to time t_i + 10 min and the value of $\bar{R}_i$ is plotted at t_i + 5 min.

The vertical distribution of liquid water generation in the mesoscale updraft was then computed for several values of t, using the distributions of ρw, RH, and θ_w. At a given value of t, the calculation was begun at the height where ρw was equal to zero. The atmosphere from there up to 8000 meters

was divided into several layers. At 8000 meters, ρw was assumed to fall to zero, based on examination of the radar echoes, which generally indicated little significant precipitation above this height. For a given layer, extending from z_i to z_{i+1}, the mass of air per hour ascending through a one m^2 cross section is

$$\dot{m}_{ai} = \overline{\rho w}_i$$

where

$$\overline{\rho w}_i = \tfrac{1}{2}(\rho w_i + \rho w_{i+1}).$$

The mixing ratio at z_i is

$$r_i = .01(RH)(r_{si})$$

where RH is the relative humidity and r_{si} is the saturation mixing ratio determined from an adiabatic chart using z_i, RH, and θ_w. The mass of vapor per hour passing through one m^2 at z_i is

$$\dot{m}_{vi} = \left(\frac{r_i}{1+r_i}\right)\dot{m}_{ai}.$$

The rate of liquid water formation within the layer is then

$$\dot{m}_{li} = \dot{m}_{vi} - \dot{m}_{vi+1}$$

In this calculation vapor is being converted to liquid at relative humidities less than 100 per cent. However, we are treating an averaged mesoscale system in which the computed RH values result from regions in which RH = 100% and liquid is being generated, in combination with regions of RH < 100% with no liquid generation. Proper determination of the averaged liquid generation dictates the approach taken here. Figure 34 presents the z-t distribution of the liquid generation rate, expressed as inches of precipitable liquid per hour per

kilometer of height. Vertical integration through this distribution expresses it as a generated rainfall rate, $R_g(t)$, shown by the solid curve in the lower half of the figure. Integration in t gives

$$\int_0^{180} R_g dt = 1.37 \text{ inches.}$$

The broken curve displays the t-variation of the averaged measured rainfall rate, $\bar{R}_m$. Its integral is

$$\int_0^{180} \bar{R}_m dt = .99 \text{ inches}$$

which agrees with the numerical average of the 42 station amounts shown on Figure 10. Thus, only 72 per cent of the generated rainfall actually reaches the ground by t = 180 min. An additional small amount falls from the anvil beyond t = 180 min. The bulk of the liquid water is generated between t = 30 and t = 100 min at heights between 2 and 4 kilometers. The region of maximum generated rainfall leads the measured rainfall maximum by fully 40 minutes. Much of the generated liquid is carried in the rearward-sloping updraft before it is able to fall out.

Estimates were made of the water vapor fluxes into and out of the storm system by integrating vertically at t = -20 min and at t = 180 min:

$$\dot{m}_v = \int \rho v_r r dz$$

where

ρ = density of air = $\rho(z)$

v_r = y-component of wind speed relative to SWS line

r = mixing ratio = $r(z, \theta_w, RH)$

and $\dot{m}_v$ is the mass flow rate of vapor through a surface

1 m wide in the x-direction.

At t = -20 the lower limit on the integral is ground level, while at t = 180 it is the height where $v_r = 0$. The upper limit is defined by the height where $\rho v_r r$ is reasonably extrapolated to zero. (Evaluation of the inflowing vapor was made at t = -20 rather than at t = 0 to make certain that the effects of the lifting at the front on the averaged variables were excluded.) Table 2 summarizes the partitioning of the vapor and liquid within the storm system. The efficiency of the system in converting all the incoming vapor into rainfall at the ground is estimated at 58 per cent. This compares well with the 60% value determined by Fankhauser (1971) for an isolated large severe storm in Texas. He assumed, however, that all of the converged water vapor was in the lowest 200 mb of the atmosphere. Using only the lowest 200 mb to evaluate the incoming vapor for this system would have given an efficiency approaching 85%. The 72% value mentioned earlier might be a more reasonable estimate for this system. A consistently calculated efficiency for this system should be higher than that for a classic severe storm. Liquid water loss due to reevaporation was probably much less in this system than in a classic storm, because the rearward shear at high levels prevented recirculation of small precipitation into the upper side of the sloping updraft. This explains the absence in the radar data of any echo overhangs above the region of low-level inflow. When an extensive overhang is present, the suspended small precipitation provides evaporative cooling for the cold,

dry mid-tropospheric air. This is the fundamental driving force of the downdrafts in severe convective storms (Hookings, 1965). This source of evaporation was absent in this case and should result in a higher efficiency for the system.

Figure 35 is a flow diagram illustrating how each 100 units of incoming water vapor is distributed by the storm system. The fact that a significant amount is allotted to storage is compatible with the observed increase in the size of the system during the time the soundings were being made.

5. CONCLUDING REMARKS

Selected results from the rawinsonde data analyses described above have been combined in Figure 36 to show how the various meteorological parameters interrelate. Indicated are the interface between the overrunning warm air and the advancing cold air, streamlines of the relative wind field, and regions of the meteorological parameters defined as follows:

1. RH > 80% (for z > 4 km)
2. RH > 90% (for z < 4 km)
3. $\sigma_{RH} > 30\%$
4. $\theta_w > 20^oC$
5. $\theta_w < 16^oC$
6. $\rho w > 1.0$ kg m^{-2} sec^{-1}
7. $R_g > .25$ in hr^{-1} km^{-1}
8. $\bar{R}_m > .8$ in hr^{-1}

The vertical exaggeration in Figure 36 is eight-to-one. The tongue of high θ_w air being forced upward by the advancing cold air is apparent in this figure. The region of maximum rainfall generation extends downwind in the average flow field from the heart of the region of large-scale saturation. The region of higher RH which is assumed associated with the anvil roughly follows the streamlines downwind from the generating precipitation.

With Figure 36 as a guide, a schematic model of this storm system was constructed, drawing upon the pertinent features of models which resulted from other investigations (Newton and Newton, 1959; Browning and Ludlum, 1962; Browning,

1964; Fankhauser, 1971). The proposed model for this storm system appears in Figure 37. This sketch, which represents an 8 to 1 vertical exaggeration of the averaged system, is probably most representative of the later stages of the system, when the main echo line was wide and was growing by the development of new cells on its forward flank. A model representing the earlier stages would show the new development to be more active and somewhat separated from the narrower main storm behind it. The anvil would be much less developed. In this model the mean wind flow as indicated by the calculated stream function has been subjectively partitioned into somewhat more erect updrafts, downdrafts, and environment air which participates in neither updrafts nor downdrafts. Solid arrows indicate the flow patterns, with broad ribbons used in selected regions to illustrate the manner in which θ_w varies along two-dimensional trajectories in the system, its value changing through entrainment and mixing. The major feature of the system is the rearward sloping updraft, a configuration which allows the generated precipitation to readily fall out and not suppress the updraft. To the rear of the storm is the weak precipitation-maintained downdraft. None of the echo overhang typically observed in severe storms (Browning 1964) appears in this system due to the fact that the upper winds shear toward the rear of the storm. As mentioned in the previous section, this prevents small precipitation from recirculating in the forward portions of the updraft and limits hail to a small size. The absence of strong surface winds in this storm

system is explained in part by the minimal amount of evaporative cooling provided to the middle-level air and the resultant lessened intensity of the downdrafts.

This storm system appears to have had little or no effect on the movement or strength of the synoptic-scale weather systems. Figure 38A displays the observed sea-level isobars and 1000 to 500-mb thickness pattern for 1200Z on May 15, about 12 hours after the storms began. Figure 38B displays the 36-hour PE prog for the same quantities, verifying at the same time. The 24- and 48- hour progs verifying at 1200Z were similar in appearance. The location of the surface low in the midwest was predicted very well. The predicted intensity of the cold air mass was slightly high, while its rate of advance was underpredicted. The storms would not be expected to affect the former, while the latter can be adequately explained by the known tendency of the PE forecast to move systems too slowly, particularly when they involve underrunning cold air. In the southern plains the 36-hour position errors are only 100 to 150 miles at most. The PE progs for vertical velocity and humidity did not indicate that such strong activity would occur in Oklahoma. They showed the major activity in Texas, where heavy rains did indeed occur. In summary, although the storm system was extensive and energetic, the subsequent movement of the frontal system was as would have been expected had the storms not occurred.

The major conclusions resulting from the analyses performed on this storm system are summarized below.

1. The storm system was strikingly linear, extending for hundreds of miles, but was only 10 to 20 miles wide on the average.
2. The system affected the NSSL mesonetwork for about four hours, producing up to two inches of rain, but the storms appeared to be marginally severe, at most.
3. The storms were definitely associated with a synoptic-scale cold front, and trailed the surface wind shift by 10 to 15 miles.
4. The convective activity developed in a region of large-scale saturation produced by forced lifting of a conditionally unstable air mass by advancing cold air. The cold air was rather shallow, so that sufficient forced lifting was accomplished well behind the surface front and rain did not commence falling at most stations until 40 to 70 minutes after the wind shift.
5. The individual storm cells traveled to the right of the winds at all levels in the overrunning warm air. This was apparently a result of the wind field configuration, as there was no evidence of storm rotation.
6. The primary contribution to the net southeastward motion of the storm line was the generation of new cells along the leading edge or up to 10 km to the southeast.
7. When the mature cells in the storm line were strong and long-lived, the developing cells often appeared as a separate and distinct new storm line, causing sharp discontinuities in the distribution of rainfall.

8. During the time the storm system was moving through the network, the width of the echo line increased greatly, responding to a major ageostrophic backing of the mid-tropospheric winds.

9. The upper-level winds carried the condensed water to the rear of the storms, beyond the rearward-sloping updraft and thus prevented any significant region of recirculating precipitation from developing. This explains the absence of large hail or of observed forward echo overhang in these storms.

10. Severe surface winds were not observed due to the combined effects of the 1-km deep layer of cold stable air beneath the storms and the absence of a region of suspended small precipitation (echo overhang) which could contribute to strong downdrafts through evaporative cooling.

11. These storms were converting about 72 per cent of the condensed water into precipitation at the ground.

12. This large, active storm system appears to have had little or no effect on the motion of synoptic-scale features.

Table 1 - Selected Rawinsonde Data

Station/Release Time		R5/1846	5A/1852	R6/1916	CHK/1945	CHK/2010	R7/2011	R7/2053
	850mb	335/ 1.9	173/ 4.3	189/ 3.7	152/ 9.9	95/ 5.5	128/ 1.4	22/ 3.3
WIND	700	154/ 4.6	202/20.9	180/ 8.3	177/15.5	191/14.6	163/13.8	174/16.3
(Dir./Speed)	600	135/ 4.3	186/15.9	182/12.8	175/11.3	169/15.9	163/18.4	169/14.7
(deg/m sec^{-1})	500	215/ 4.3	196/17.8	201/11.9	187/17.5	170/ 8.0	156/ 8.7	170/12.0
	400	235/11.0	208/15.7	228/15.9	203/10.8	187/ 9.2	163/ 7.7	166/18.4
	850	67	85	95	96	98	100	97
RELATIVE	700	62	98	100	100	100	98	70
HUMIDITY	600	61	100	98	90	100	100	69
(per cent)	500	76	90	100	100	94	100	81
	400	78	77	78	93	81	72	82
WET-BULB	850	18.8	20.5	20.8	20.6	20.3	20.0	19.0
POTENTIAL	700	17.5	18.0	18.7	20.7	19.8	18.4	16.7
TEMPERATURE	600	18.2	18.8	18.5	18.1	20.4	19.2	16.7
(^{o}C)	500	19.9	18.0	23.9	22.0	19.5	21.8	18.1
	400	19.3	18.3	22.2	25.0	19.4	21.3	18.8
P AT WIND SHIFT LEVEL		800mb	895	890	900	850	870	840

TABLE 2

Two-Dimensional System Water Budget

		($kg\ m^{-1}hr^{-1}$)
1.	Water vapor flux into system	1.04×10^6
2.	Liquid water generation	$.84 \times 10^6$
3.	Measured precipitation	$.60 \times 10^6$
4.	Water vapor flux out of system	$.33 \times 10^6$
5.	Water vapor not condensed (=1-2)	$.20 \times 10^6$
6.	Reevaporated water (=4-5)	$.13 \times 10^6$
7.	Storage (=1-3-4)	$.11 \times 10^6$

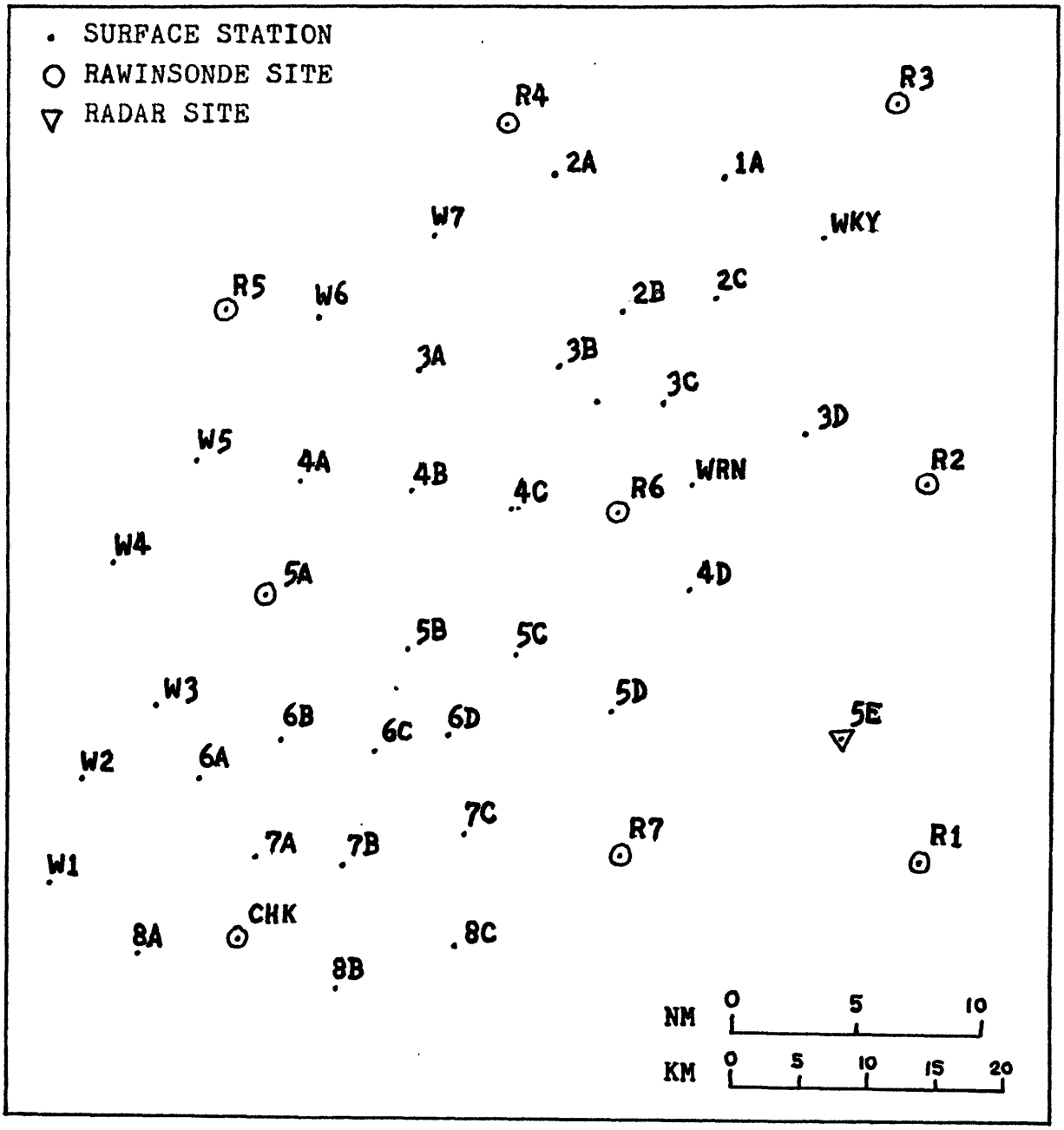

FIGURE 1 - THE 1970 NSSL MESONETWORK

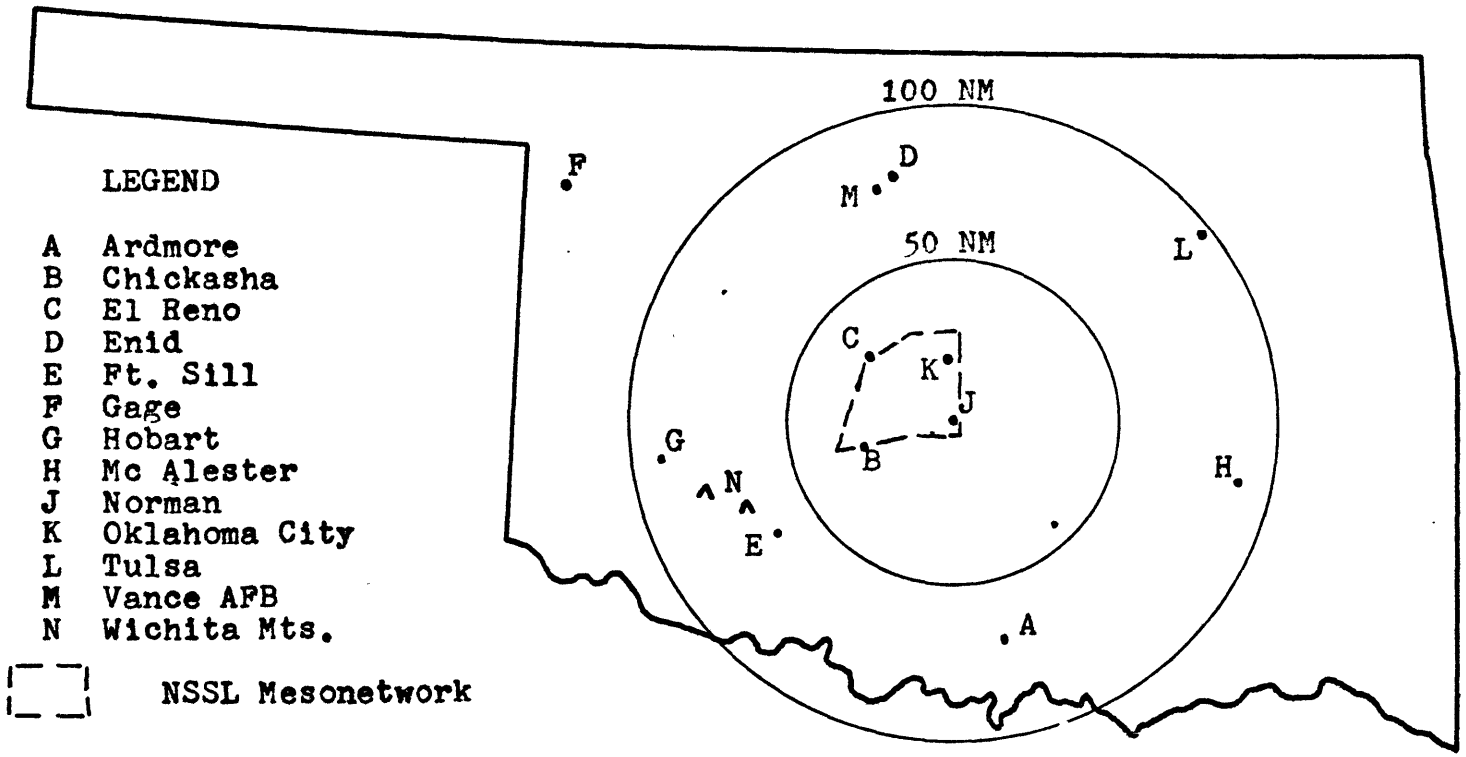

FIGURE 2 - Selected Oklahoma Observing Sites, the Location of the NSSL Mesonetwork, and Range Lines for its Radar

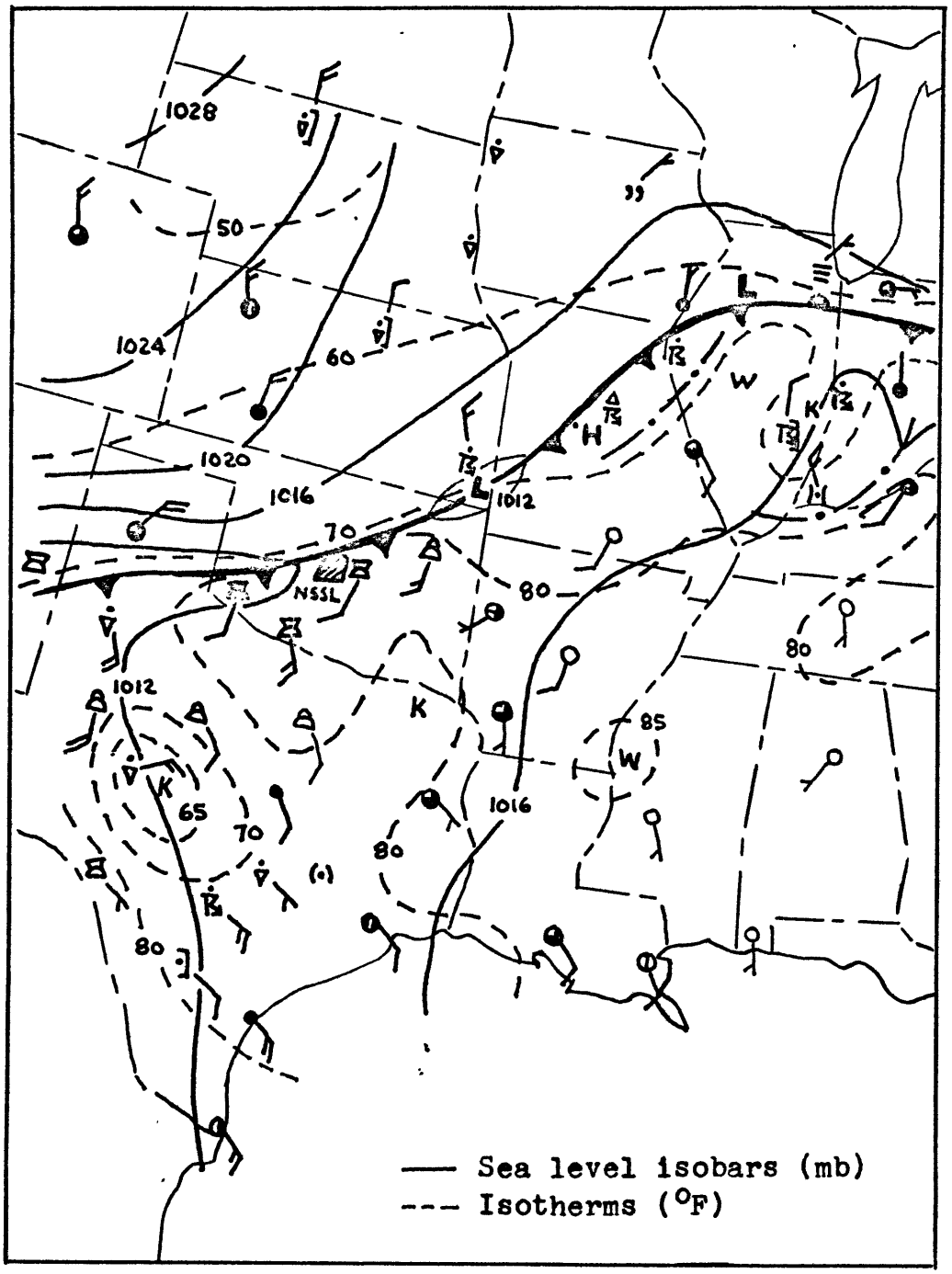

FIGURE 3 - Surface Analysis at 1800 CST, 14 May 1970

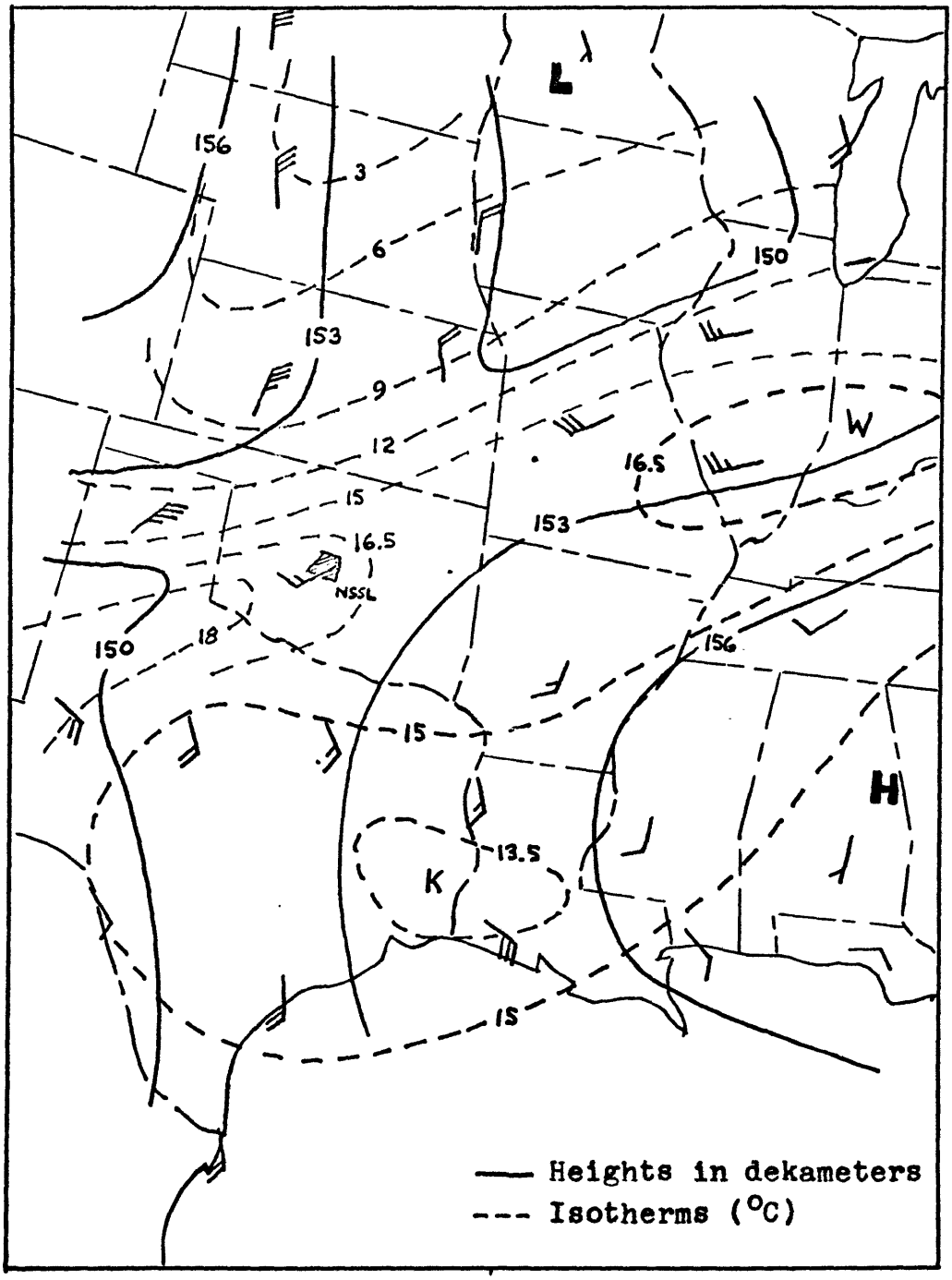

FIGURE 4 - The 850-mb Analysis at 1800 CST, 14 May 1970

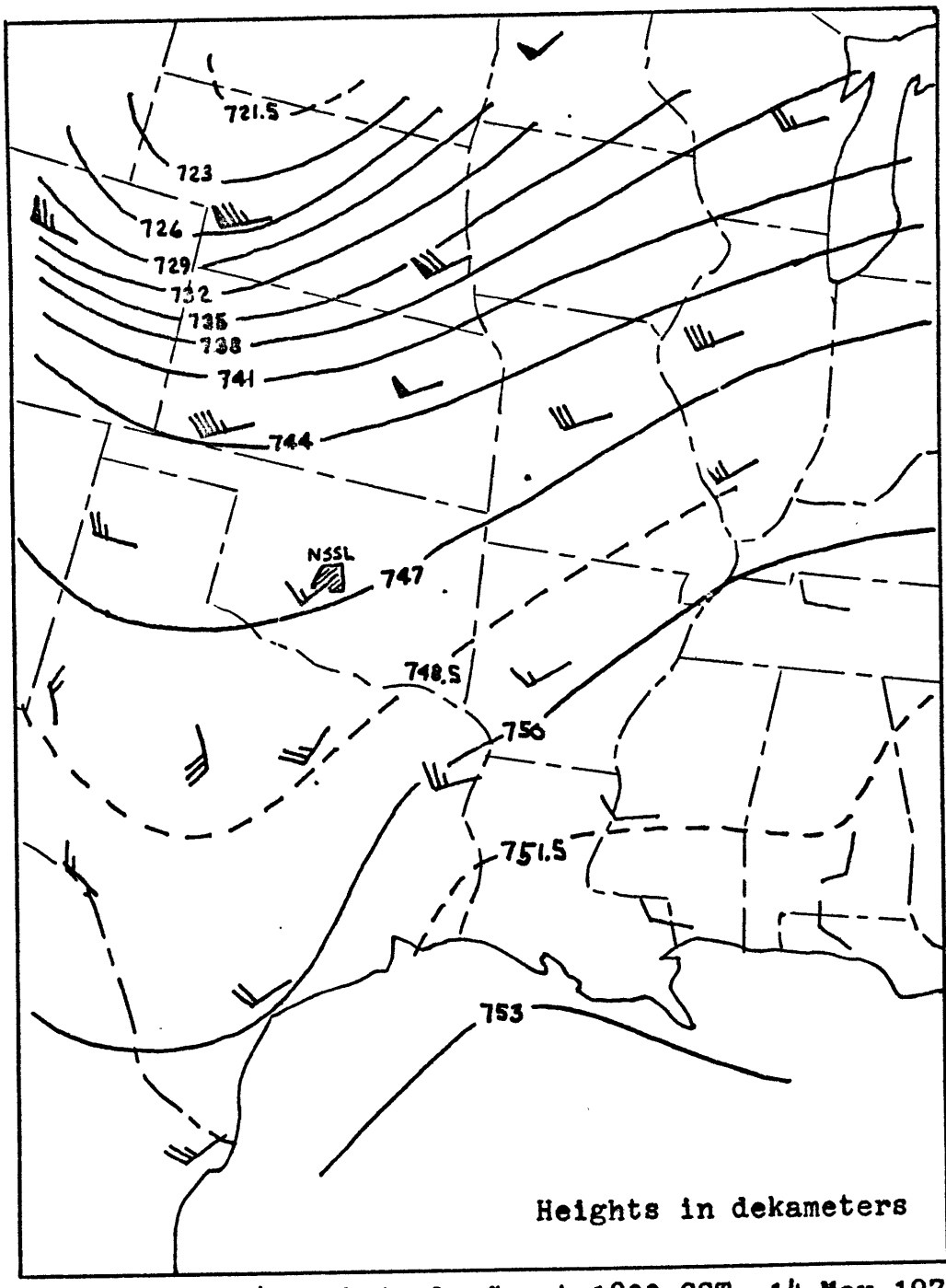

FIGURE 5 - The 400-mb Analysis at 1800 CST, 14 May 1970

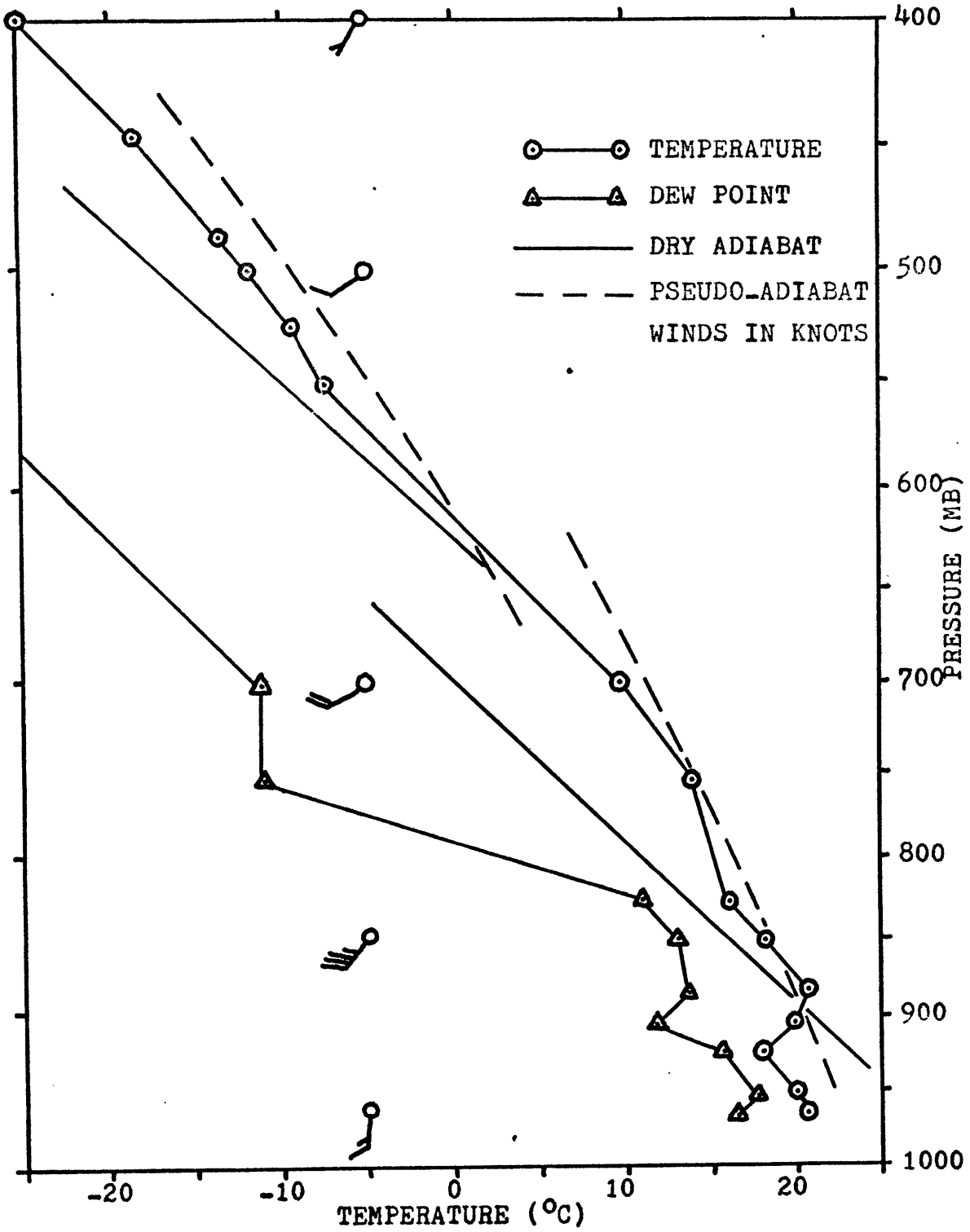

FIGURE 6 - Oklahoma City Sounding at 0600 CST, 14 May 1970

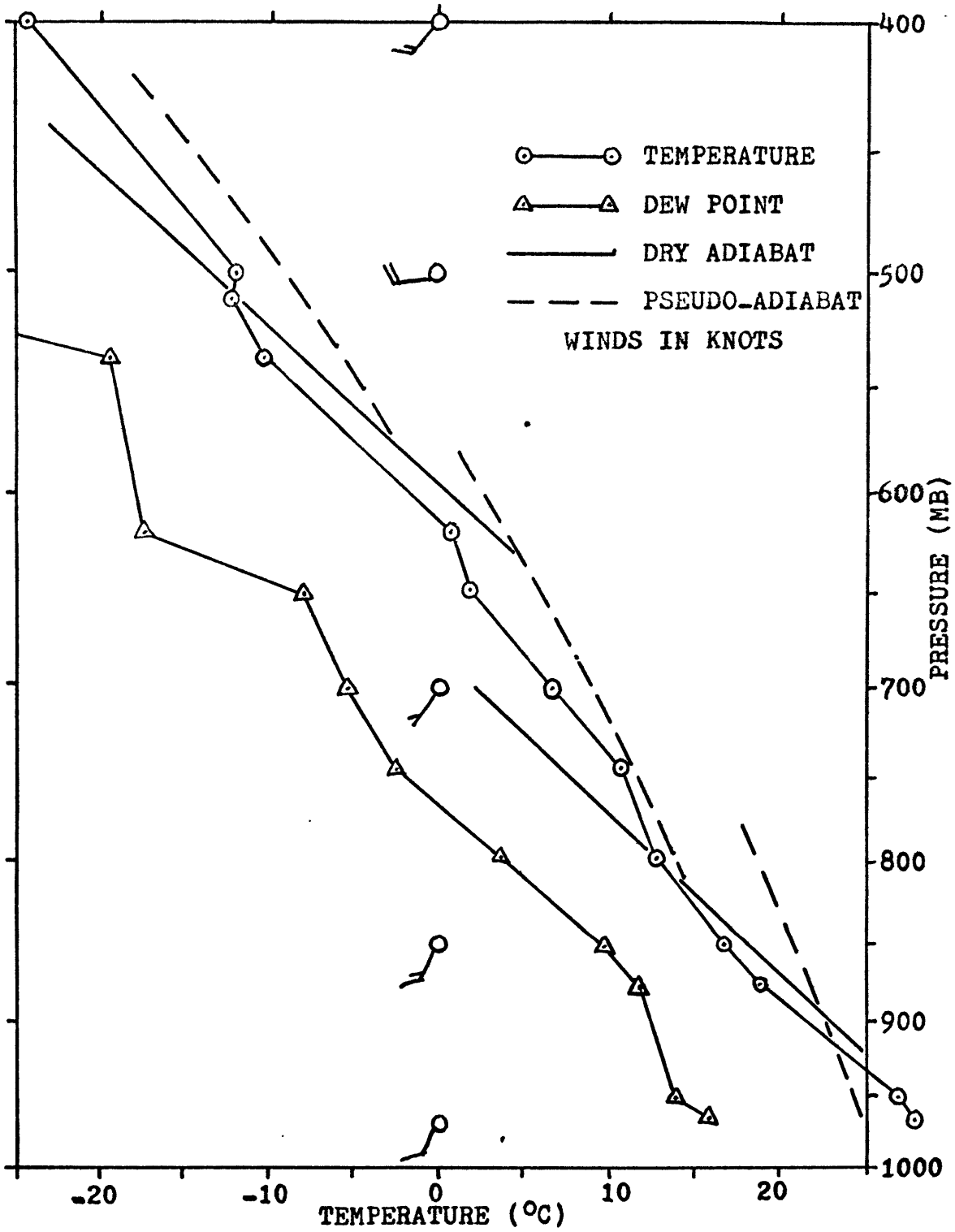

FIGURE 7 - Oklahoma City Sounding at 1800 CST, 14 May 1970

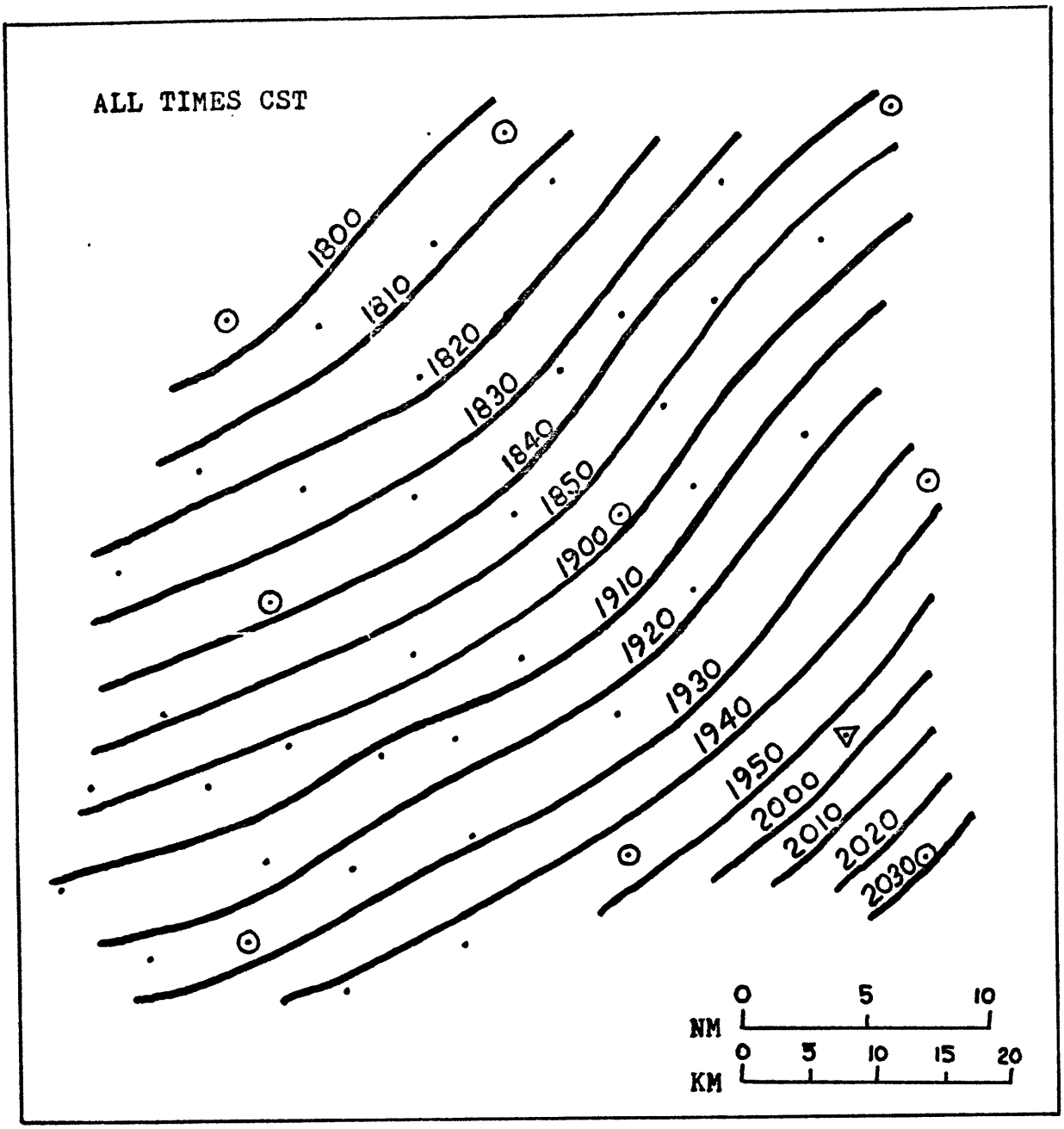

FIGURE 8 - Movement of Surface Wind Shift Line

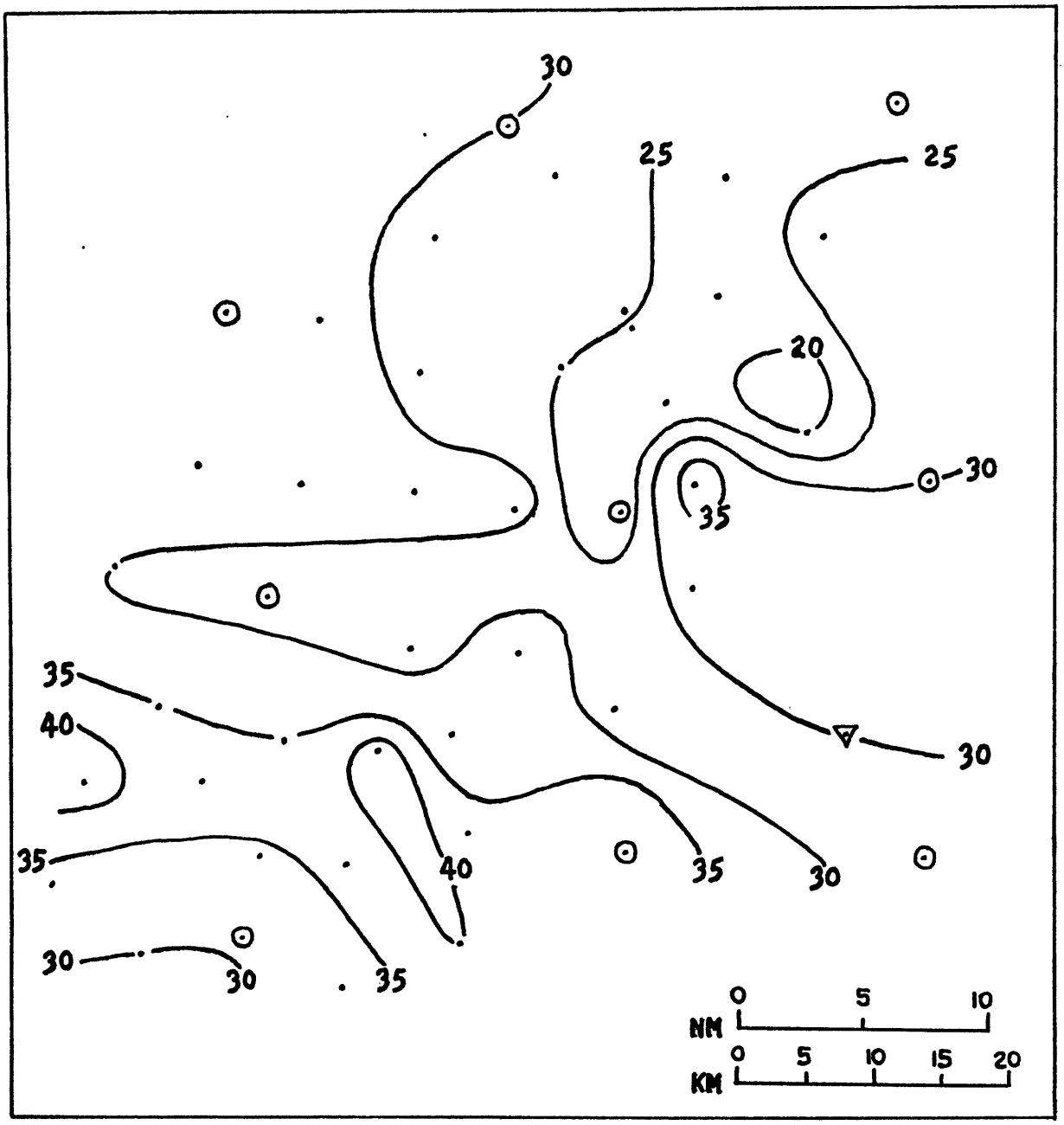

FIGURE 9 - Maximum Wind Gusts (Knots)

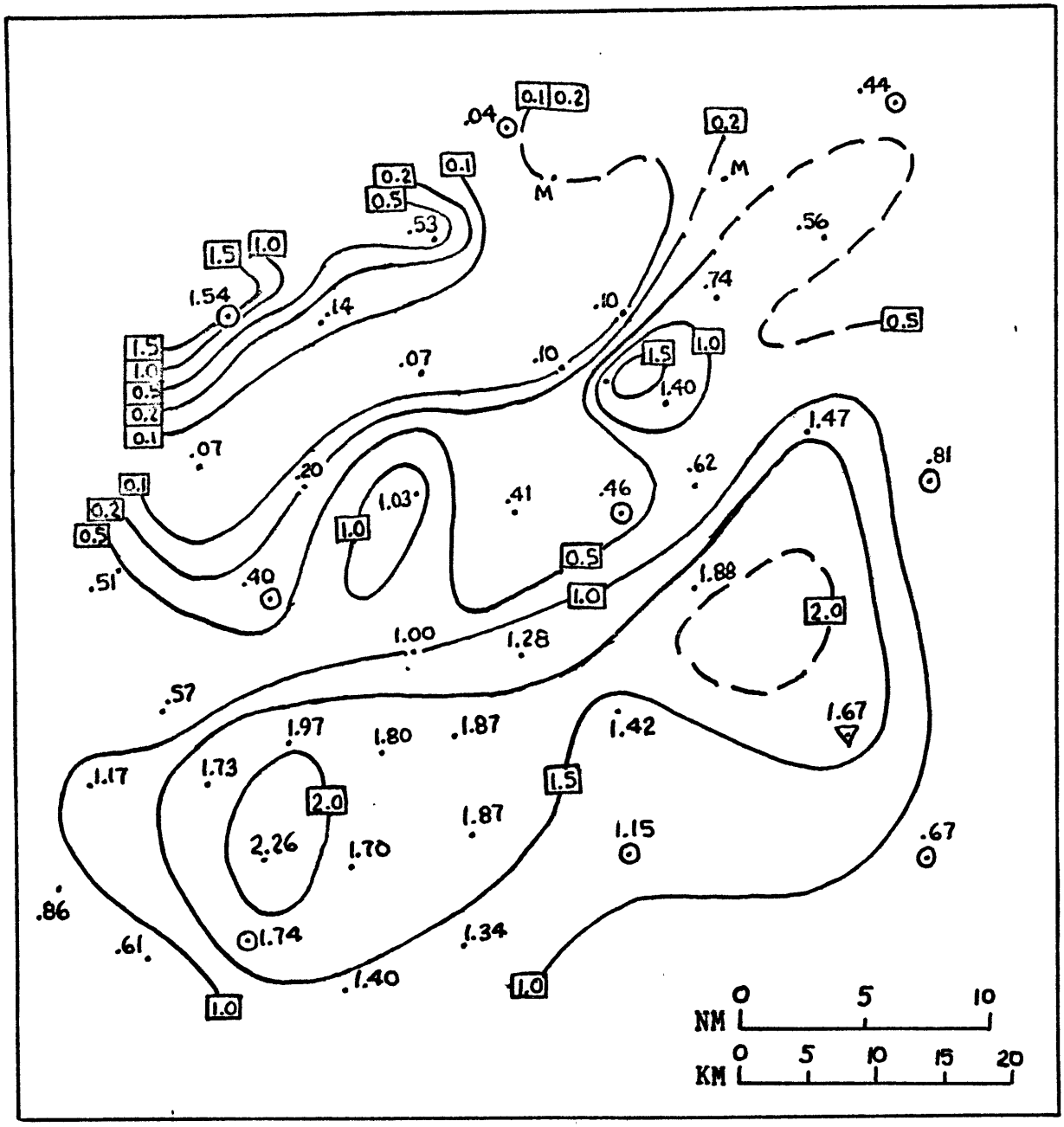

FIGURE 10 - Total Precipitation at Each Station in the Three-Hour Period Following Surface Wind Shift Line Passage (Inches)

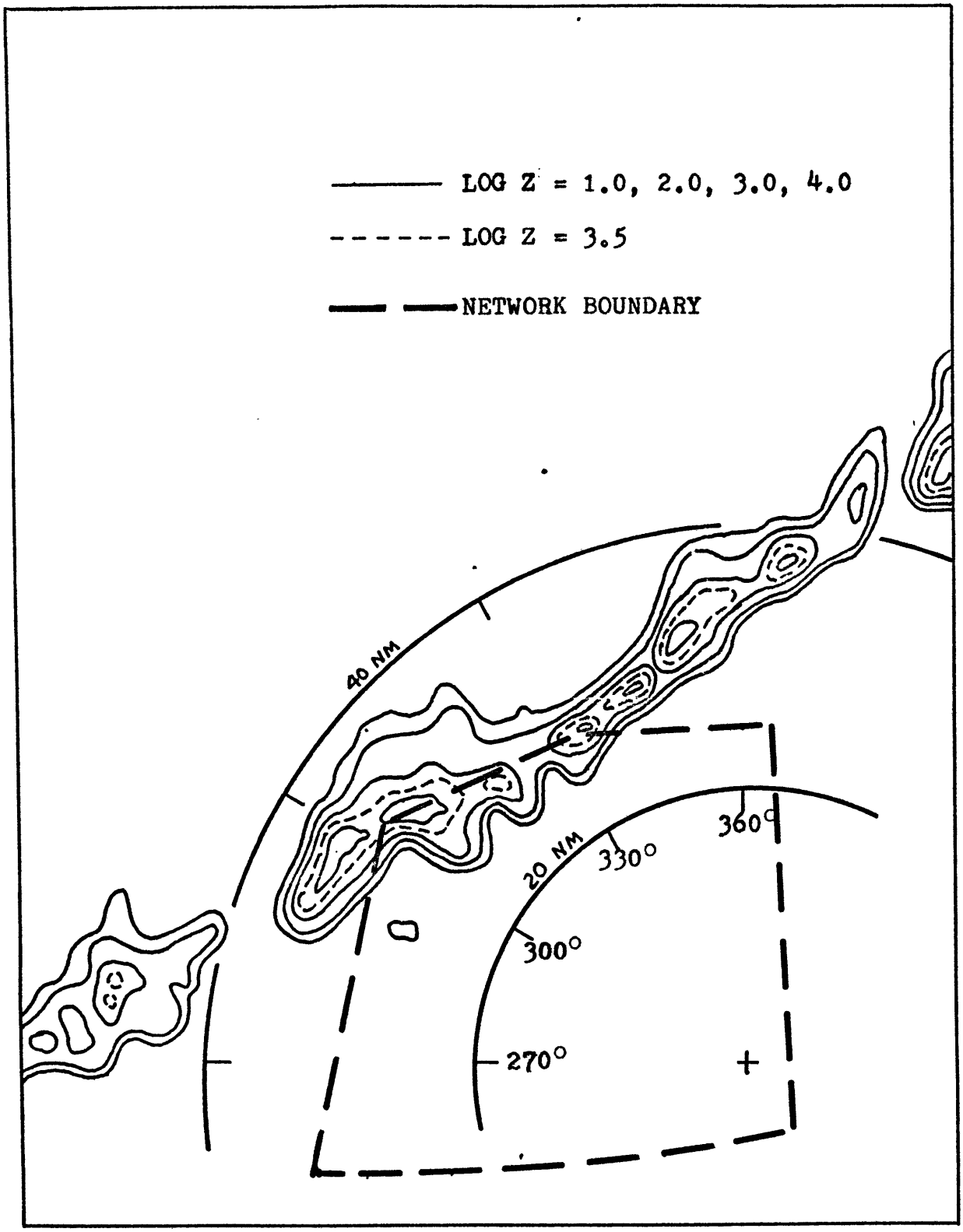

FIGURE 11 - ZERO-ELEVATION PPI DISPLAY AT 1900 CST

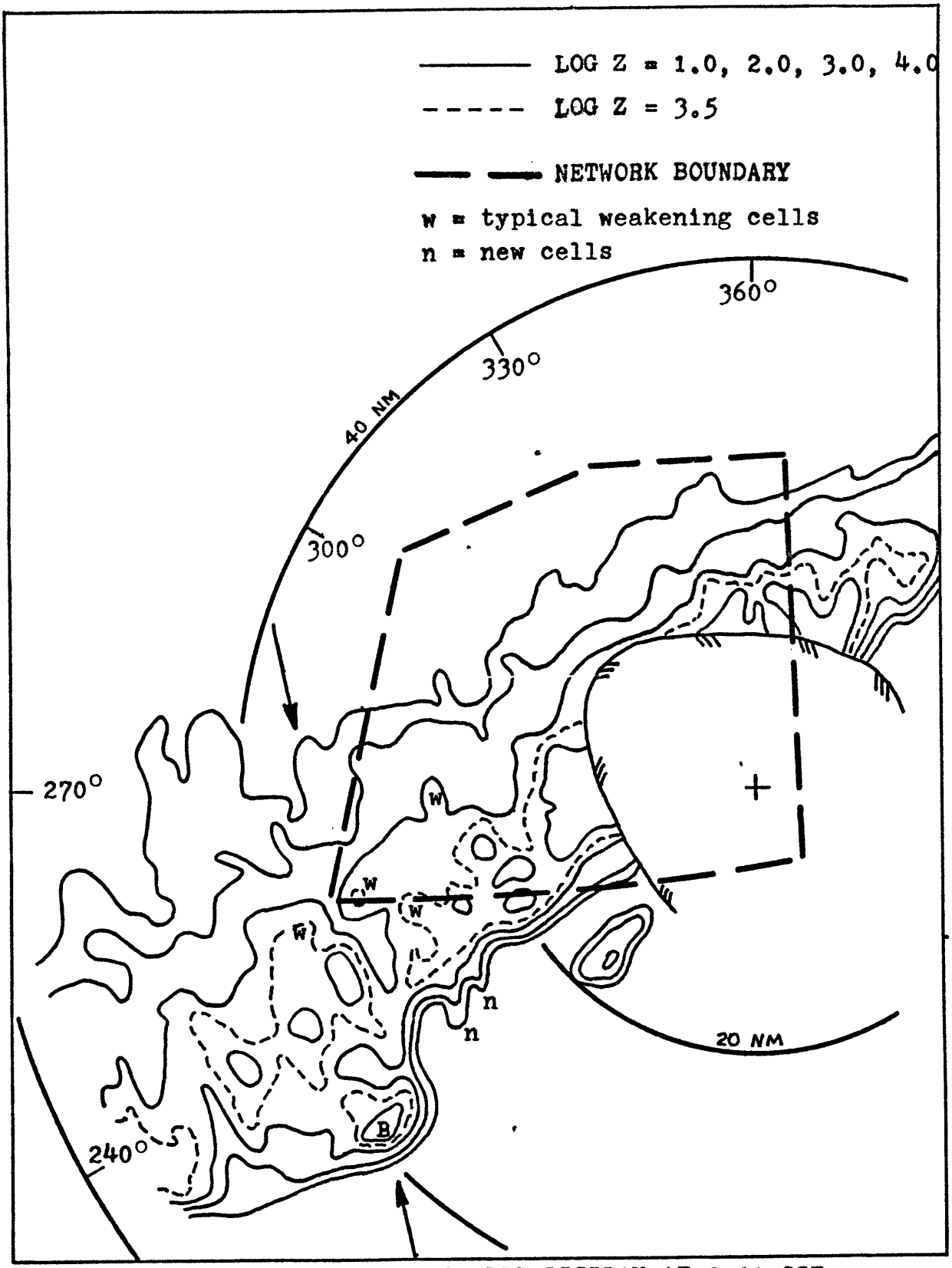

FIGURE 12 - ZERO-ELEVATION PPI DISPLAY AT 2100 CST

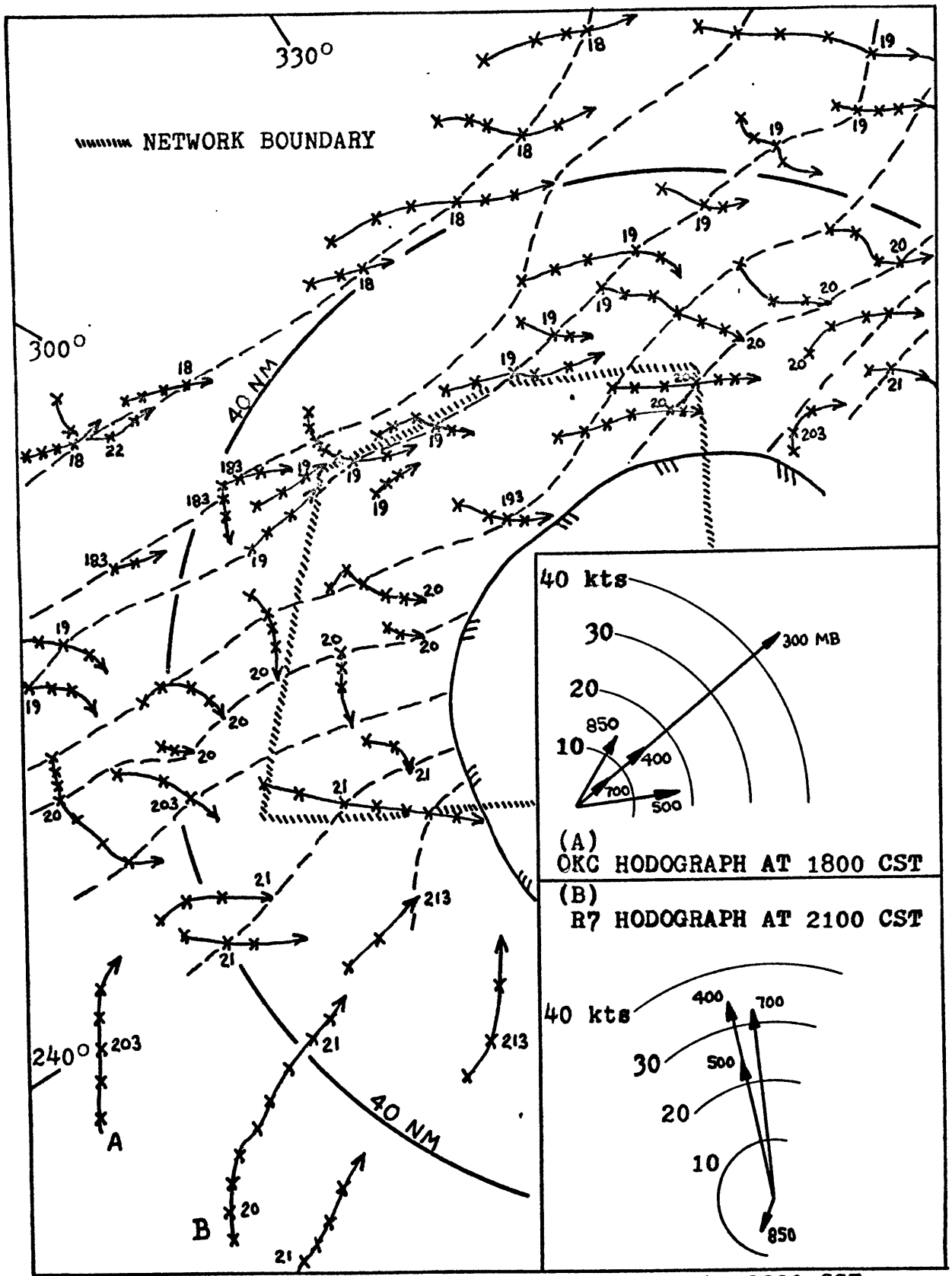

FIGURE 13 - Tracks of Storm Cells From 1730 to 2220 CST and Wind Hodographs at 1800 and 2100 CST

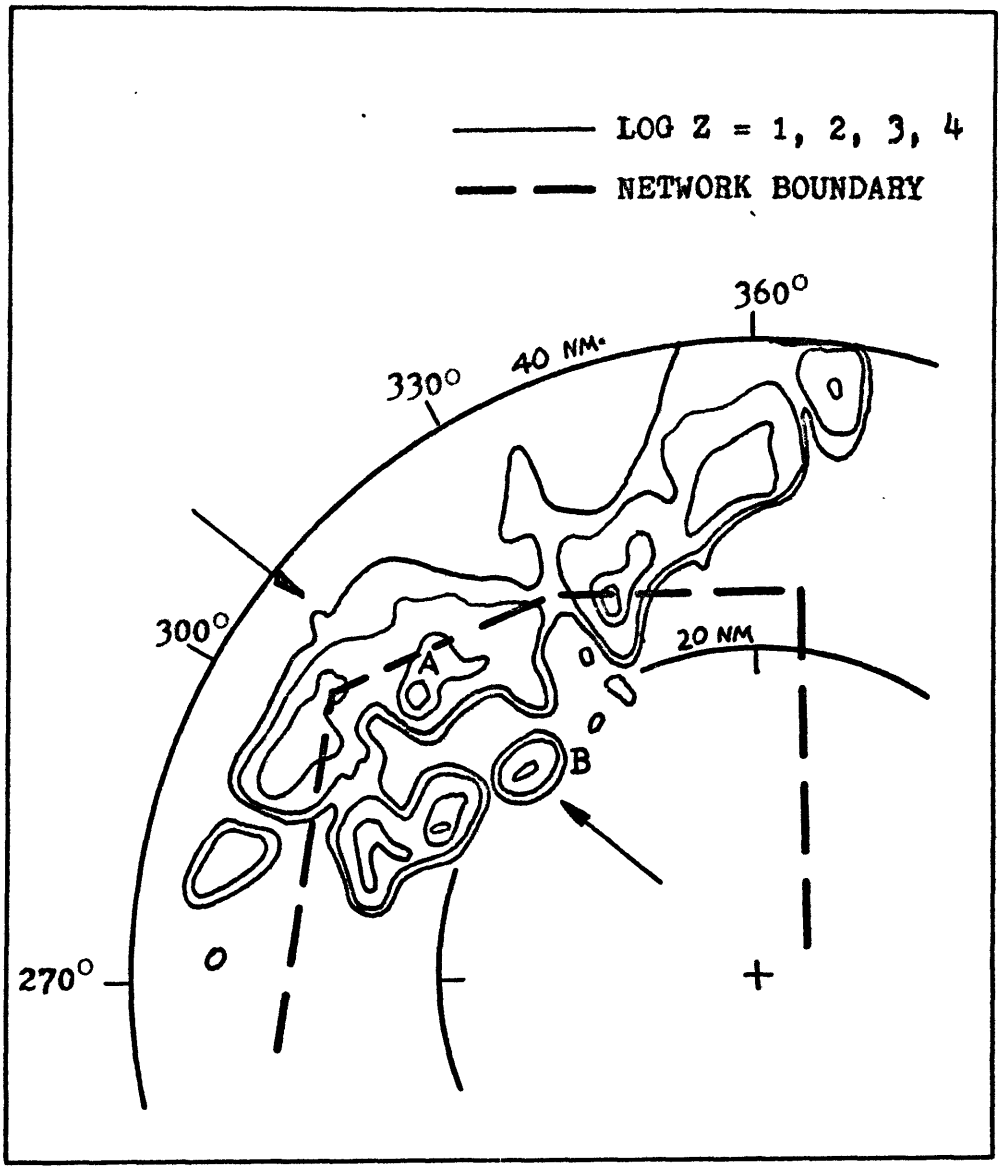

FIGURE 14 - PPI Display at 1910 CST, 4° Elevation

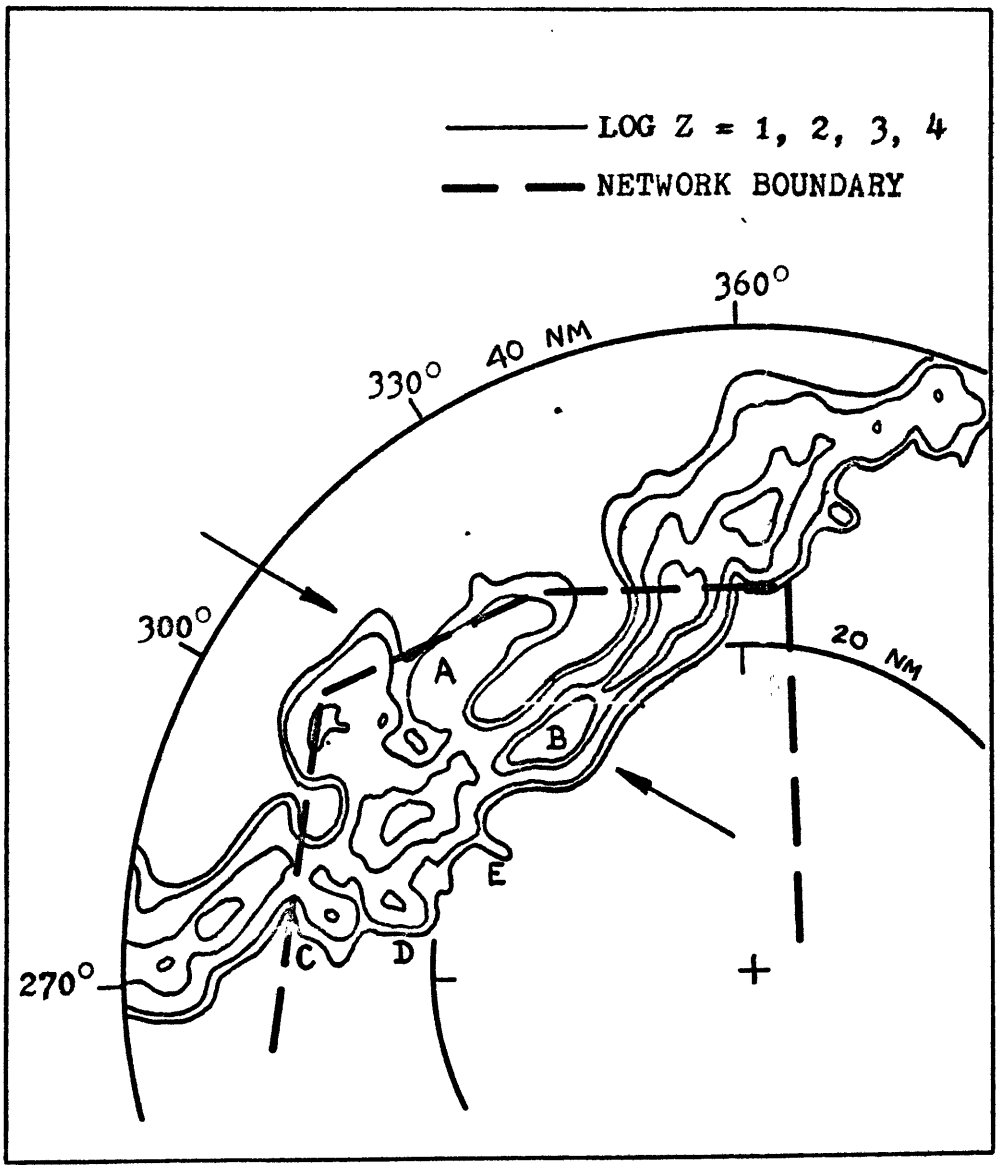

FIGURE 15 - PPI Display at 1930 CST,
2^{o} Elevation

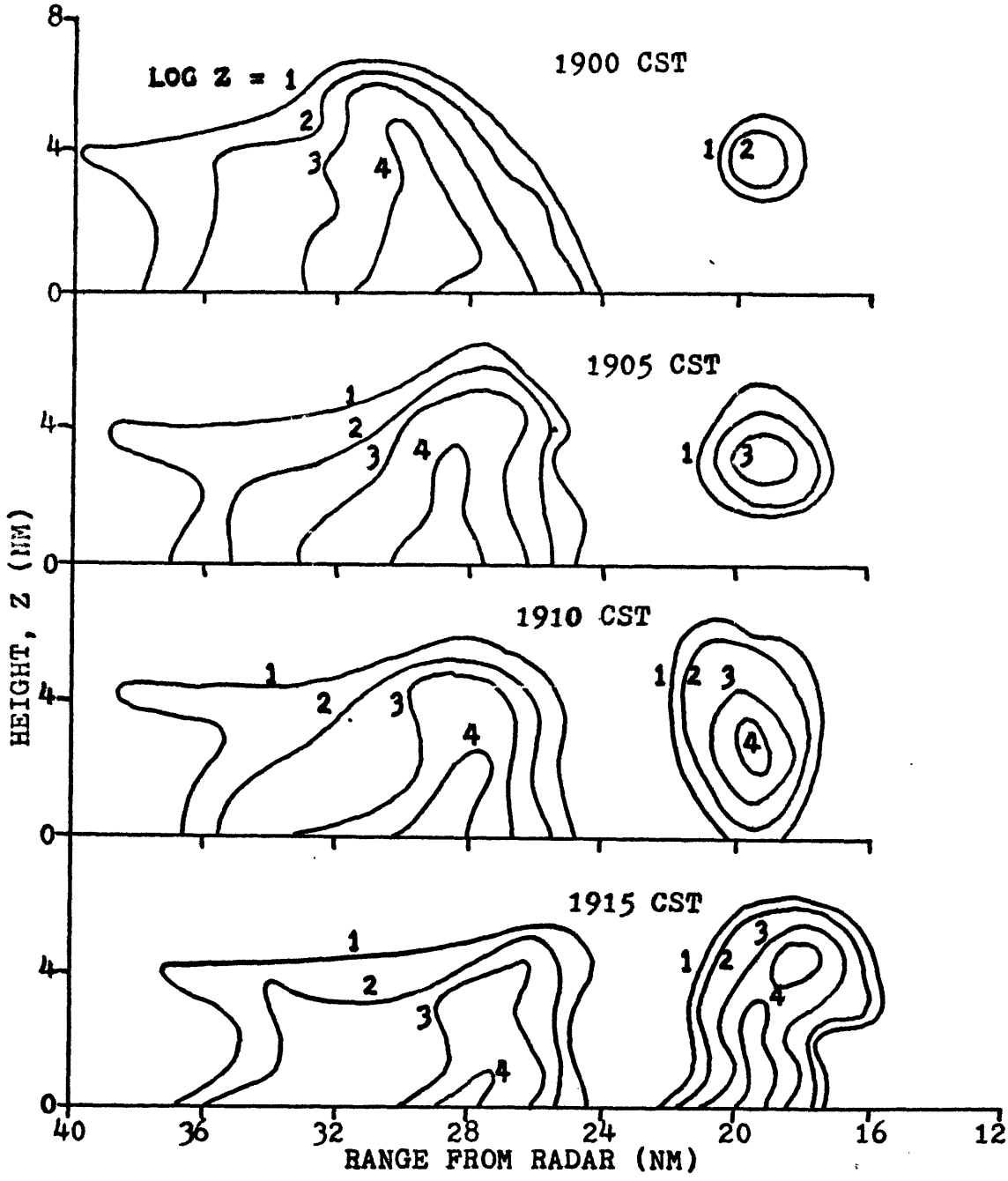

FIGURE 16 - Transverse Cross-Sections Showing Redevelopment of Storm Line

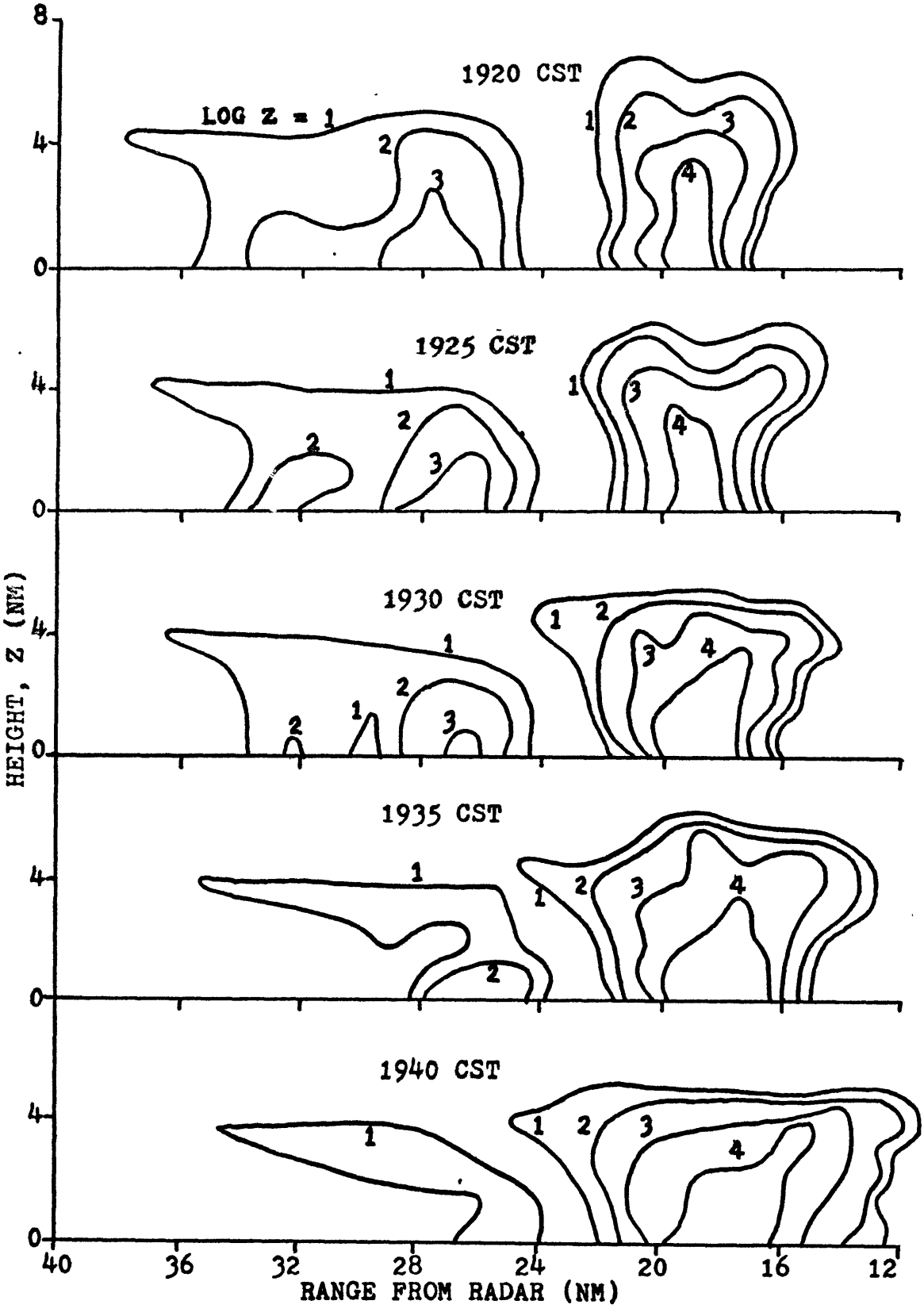

FIGURE 16 (Concluded)

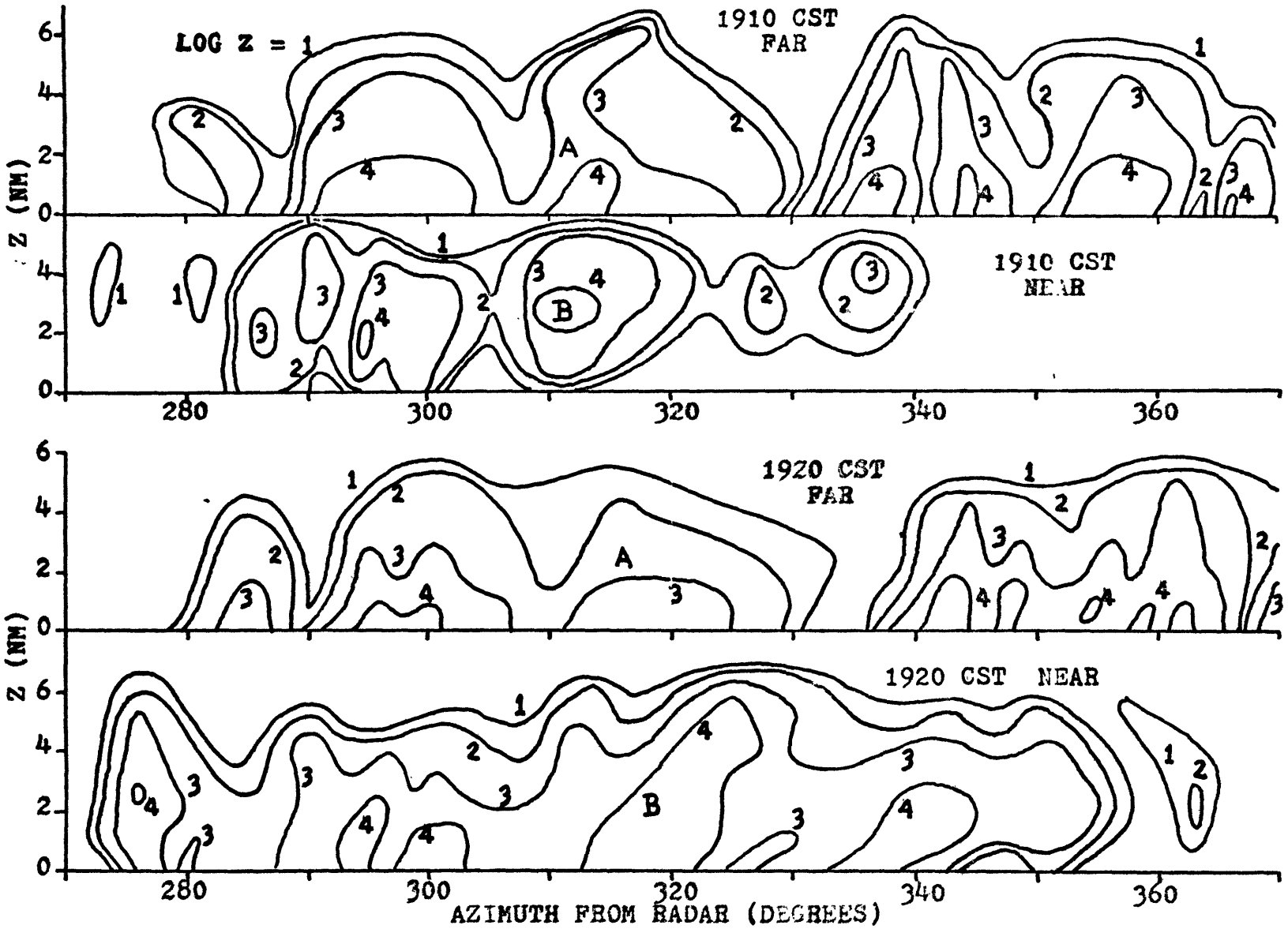

FIGURE 17 - Longitudinal Cross-Sections Showing Redevelopment of Storm Line

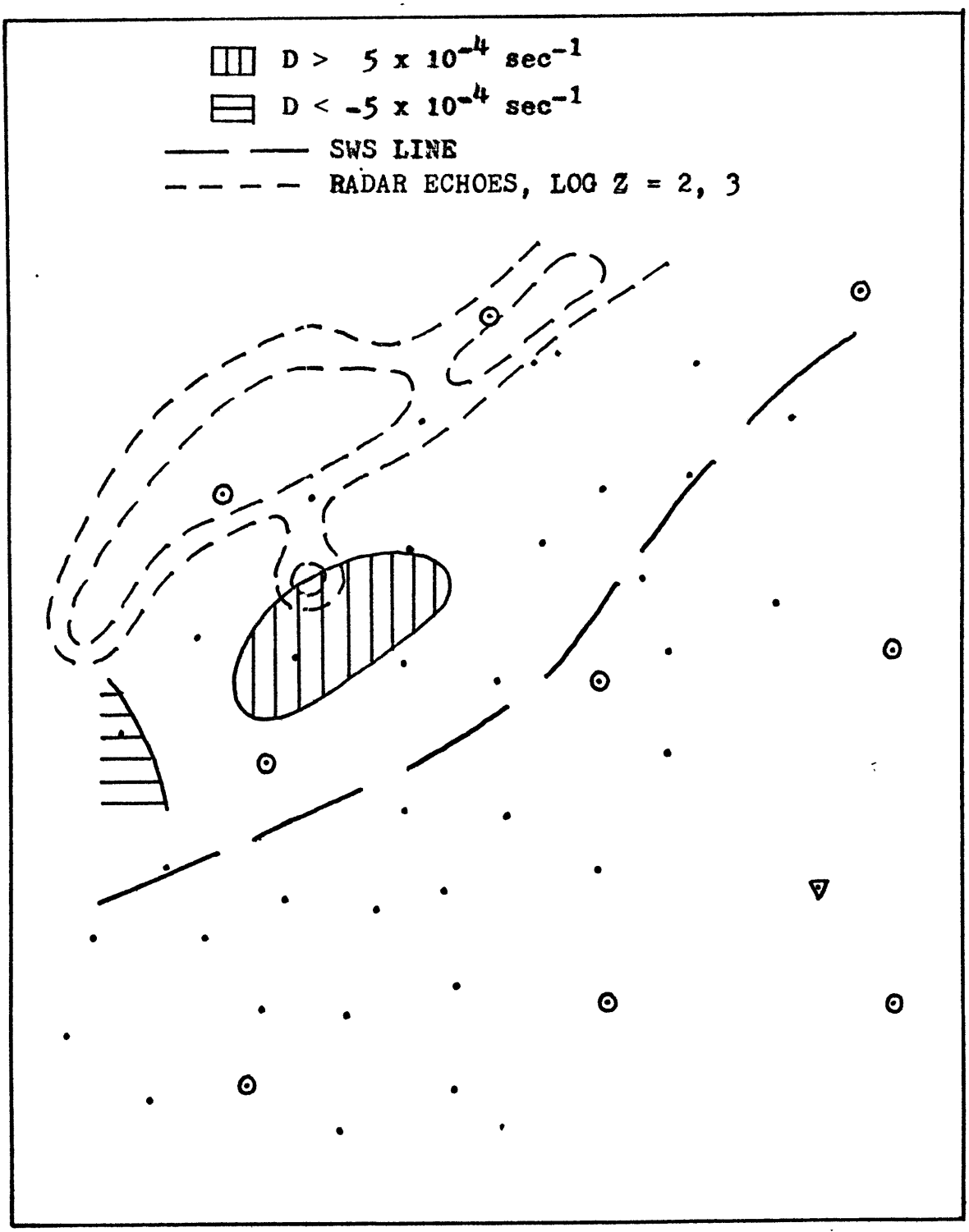

FIGURE 18 - Divergence of Surface Wind Field at 1850 CST

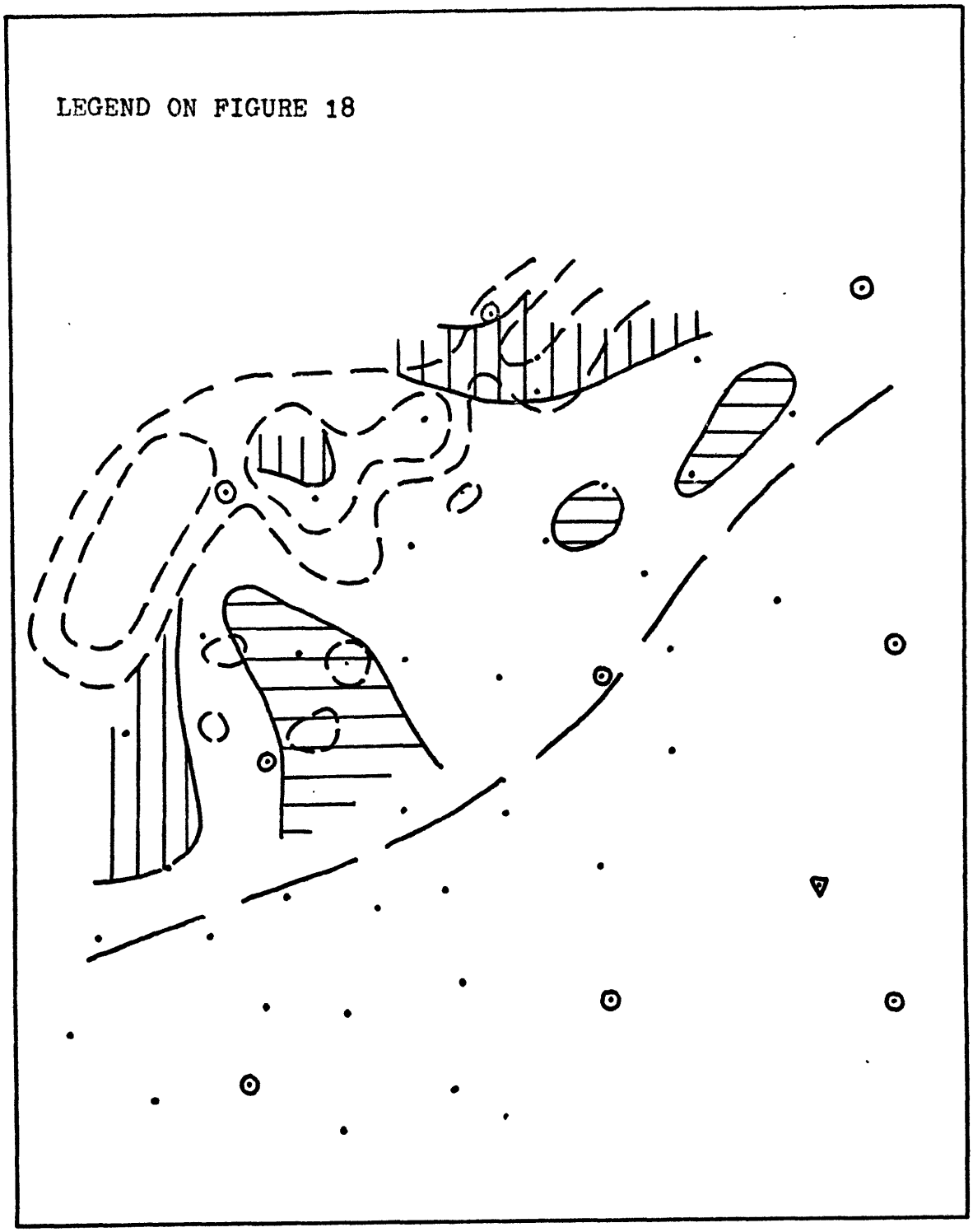

FIGURE 19 - Divergence of Surface Wind Field at 1900 CST

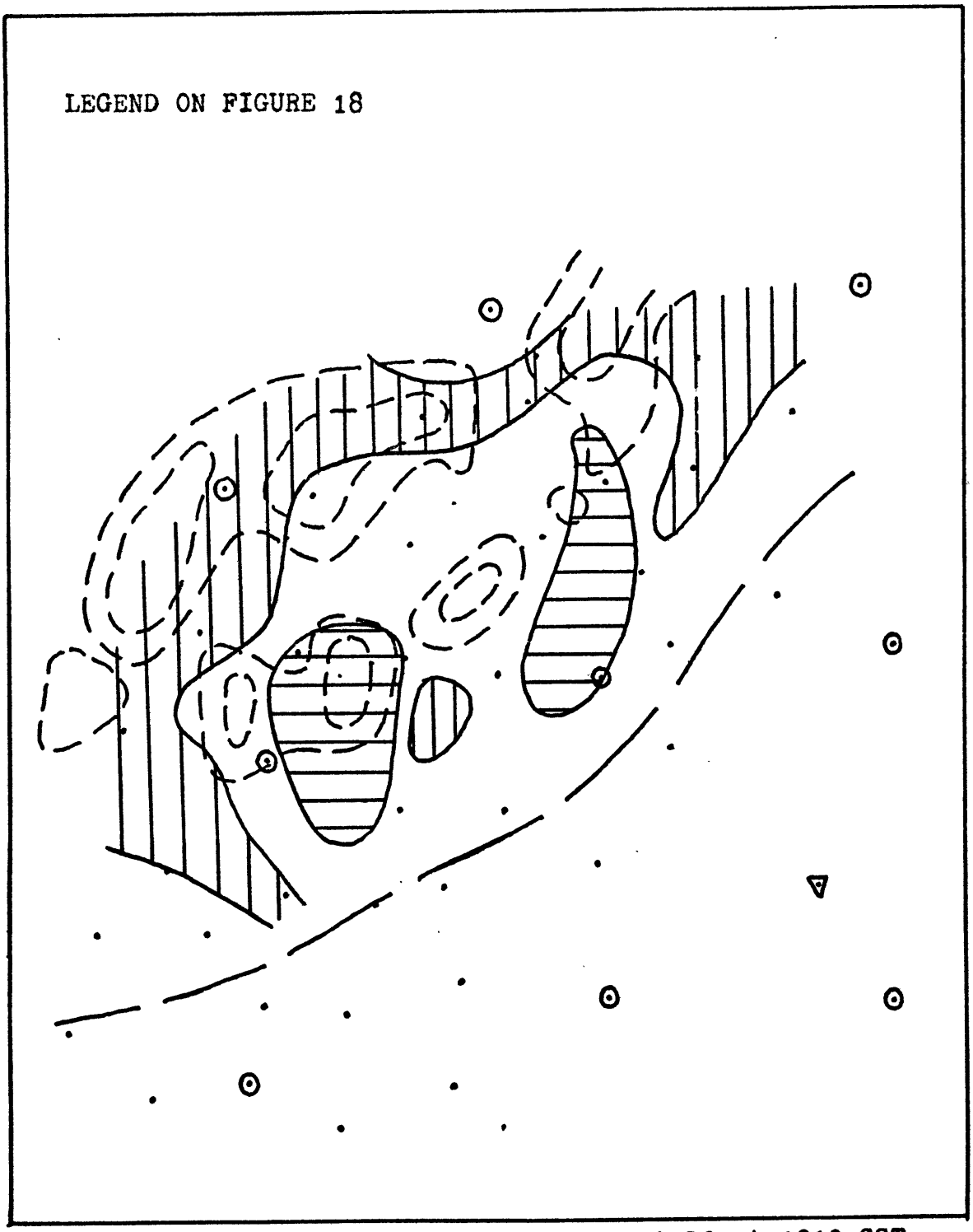

FIGURE 20 - Divergence of Surface Wind Field at 1910 CST

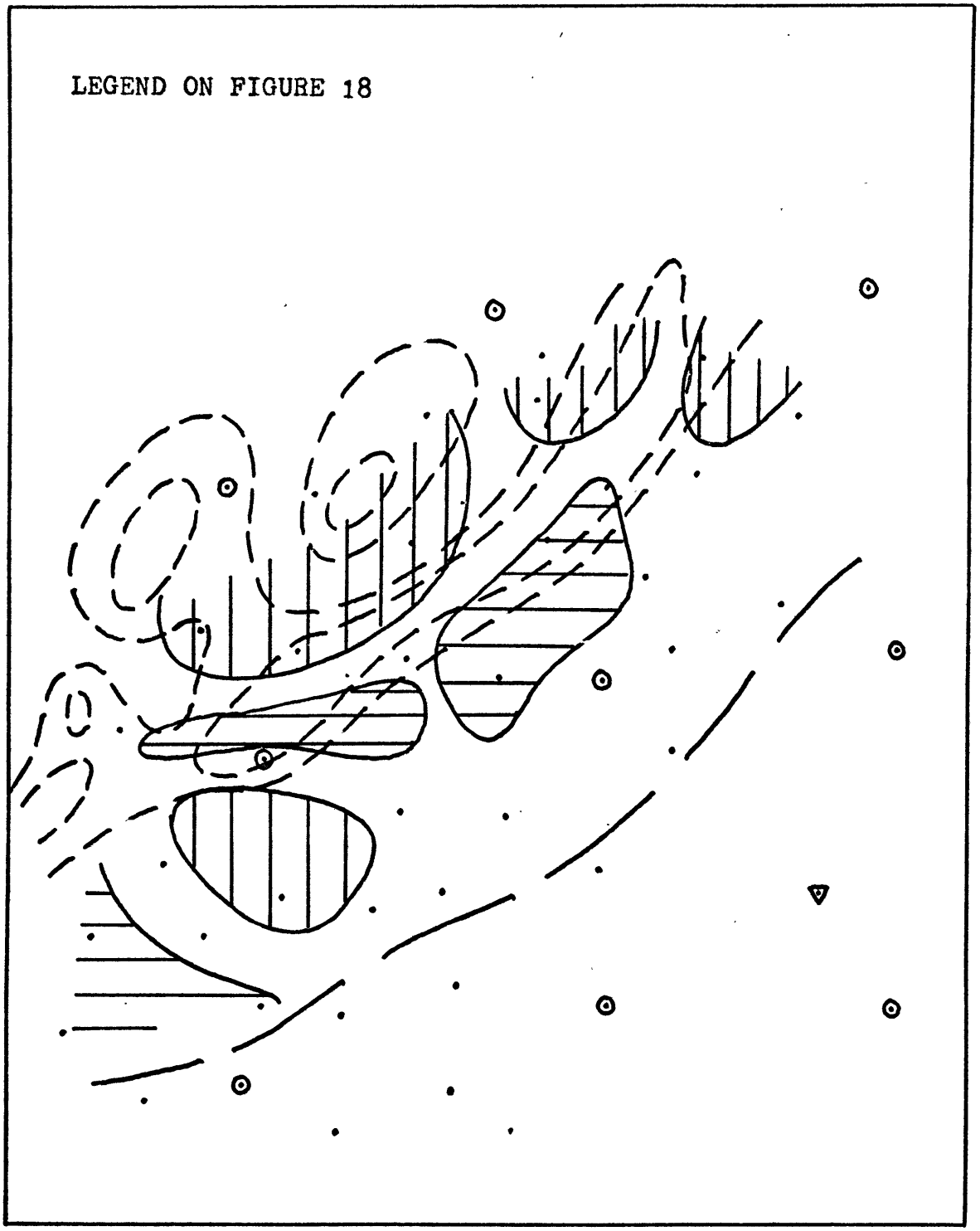

FIGURE 21 - Divergence of Surface Wind Field at 1920 CST

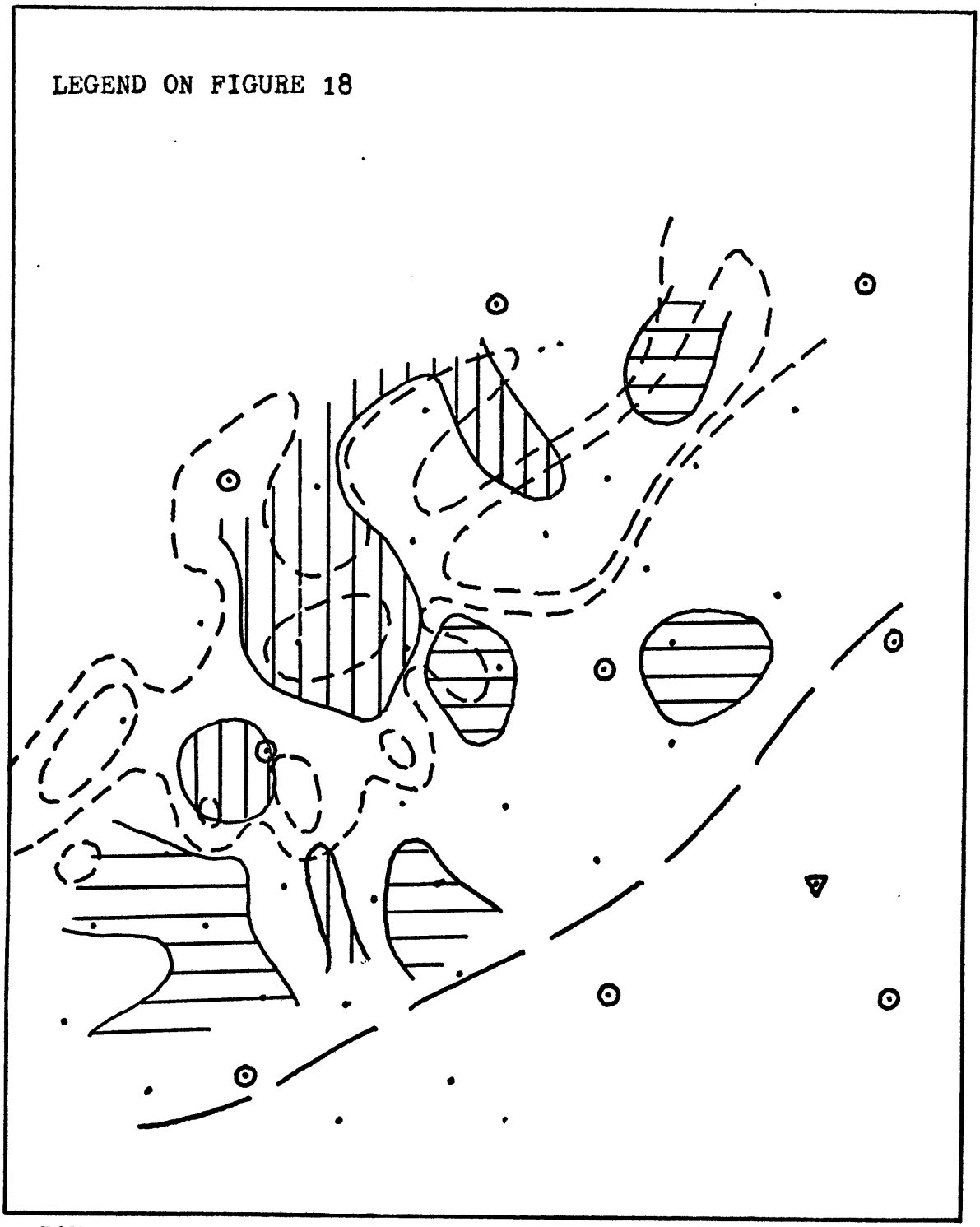

FIGURE 22 - Divergence of Surface Wind Field at 1930 CST

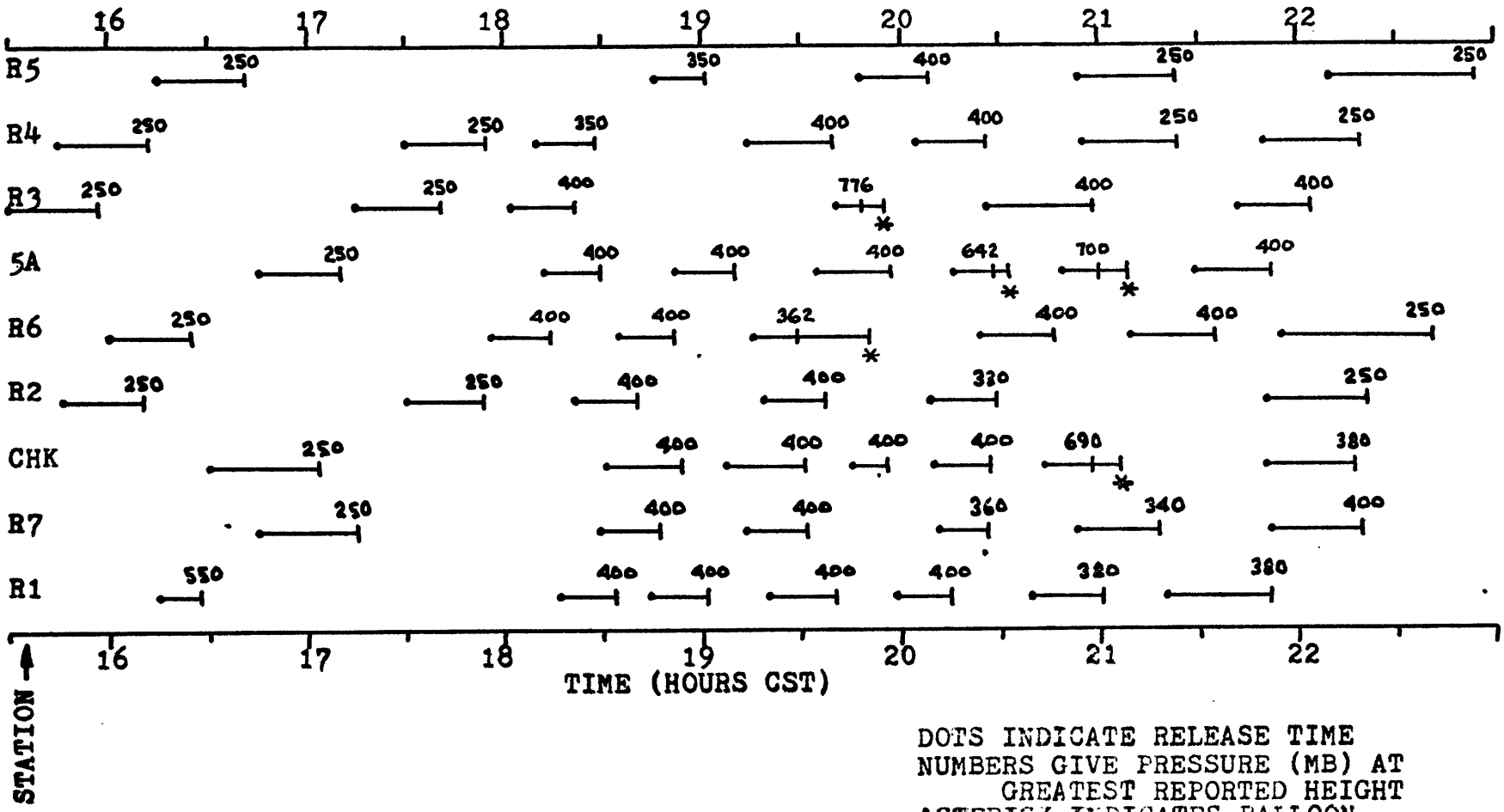

FIGURE 23 - Summary of Rawinsonde Ascents, 14 May 1970

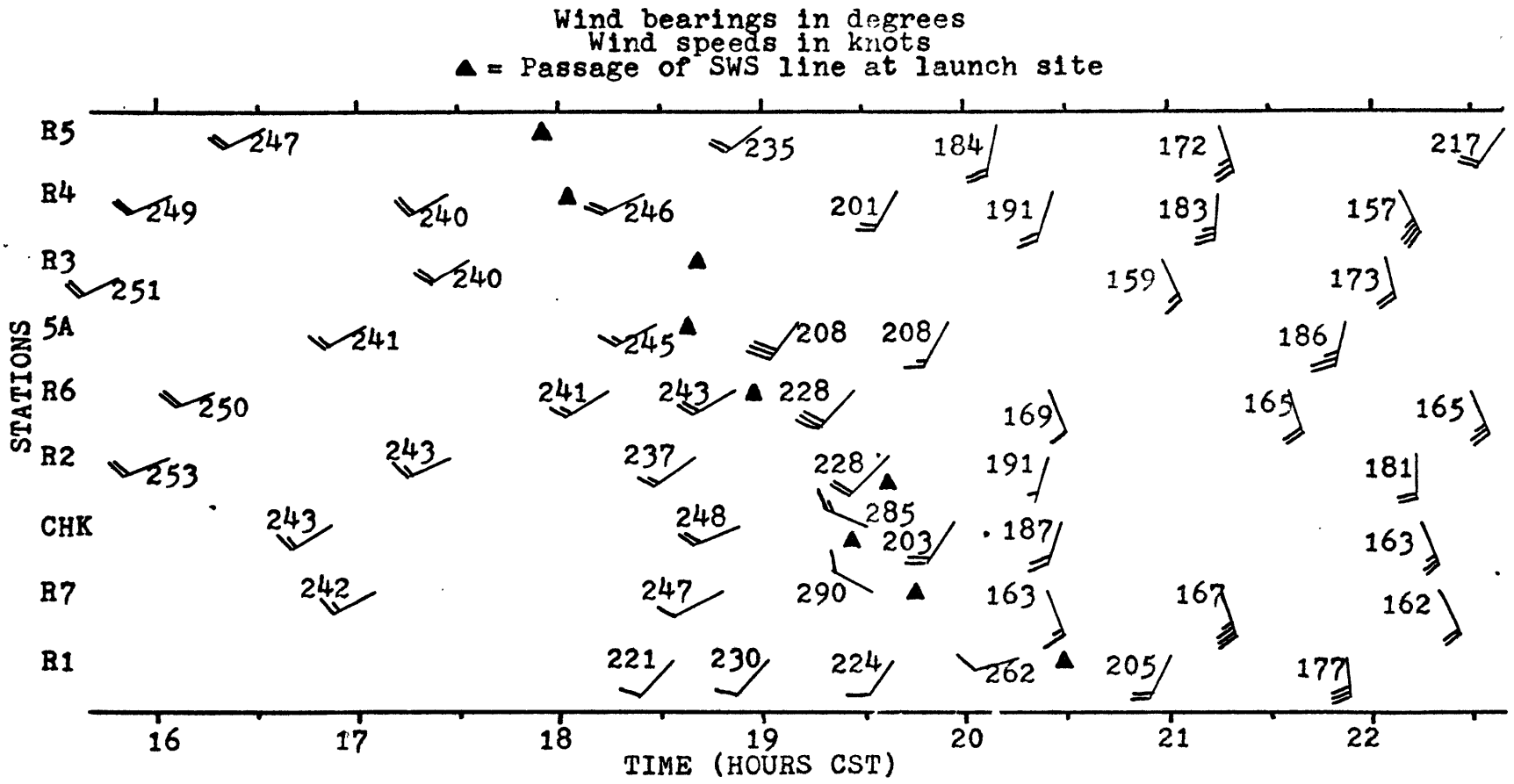

FIGURE 24 - Time Series of 400-mb Wind Observations

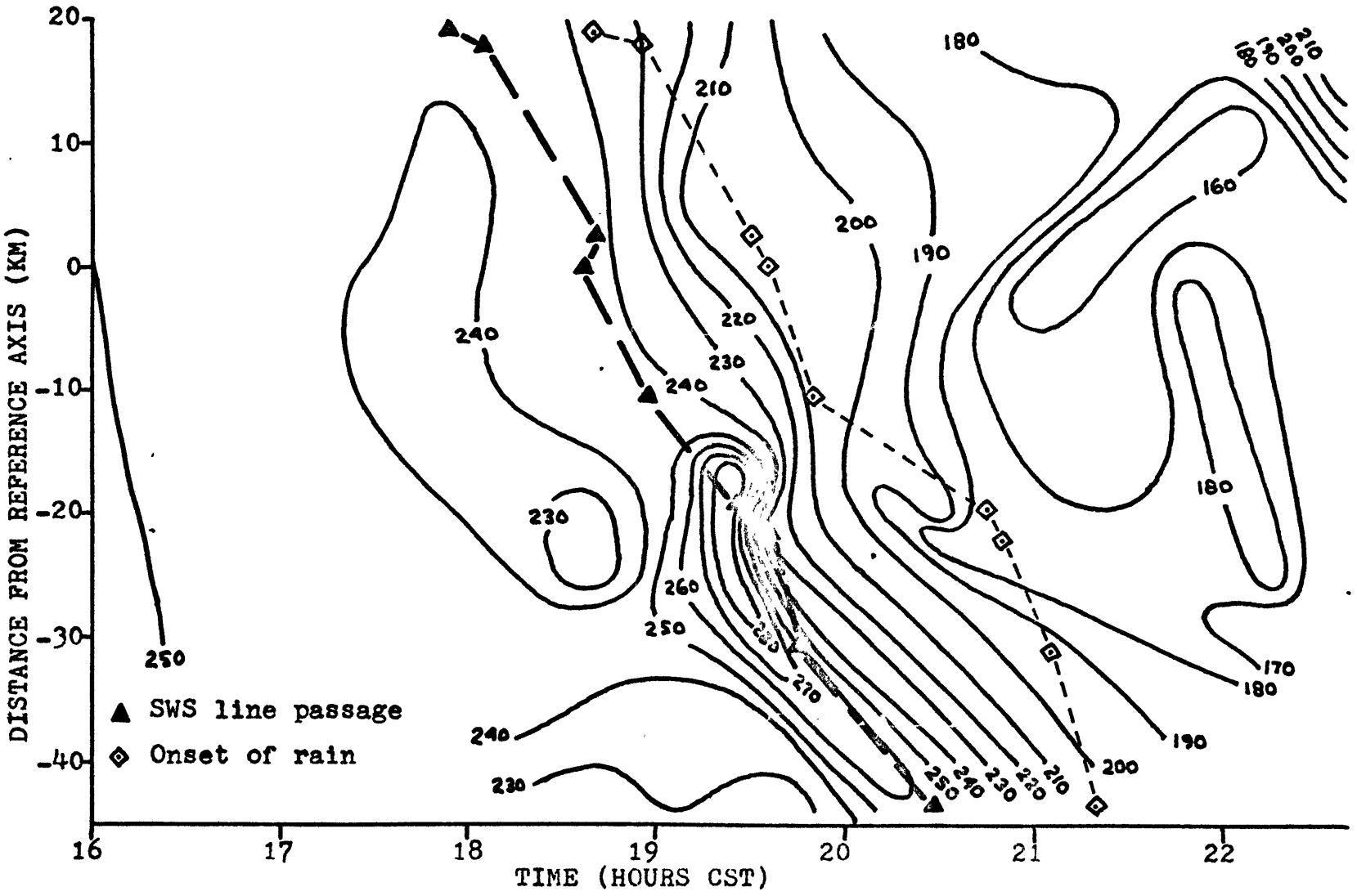

FIGURE 25 - Development of Backing in the 400-mb Wind Field (Isogons in Degrees)

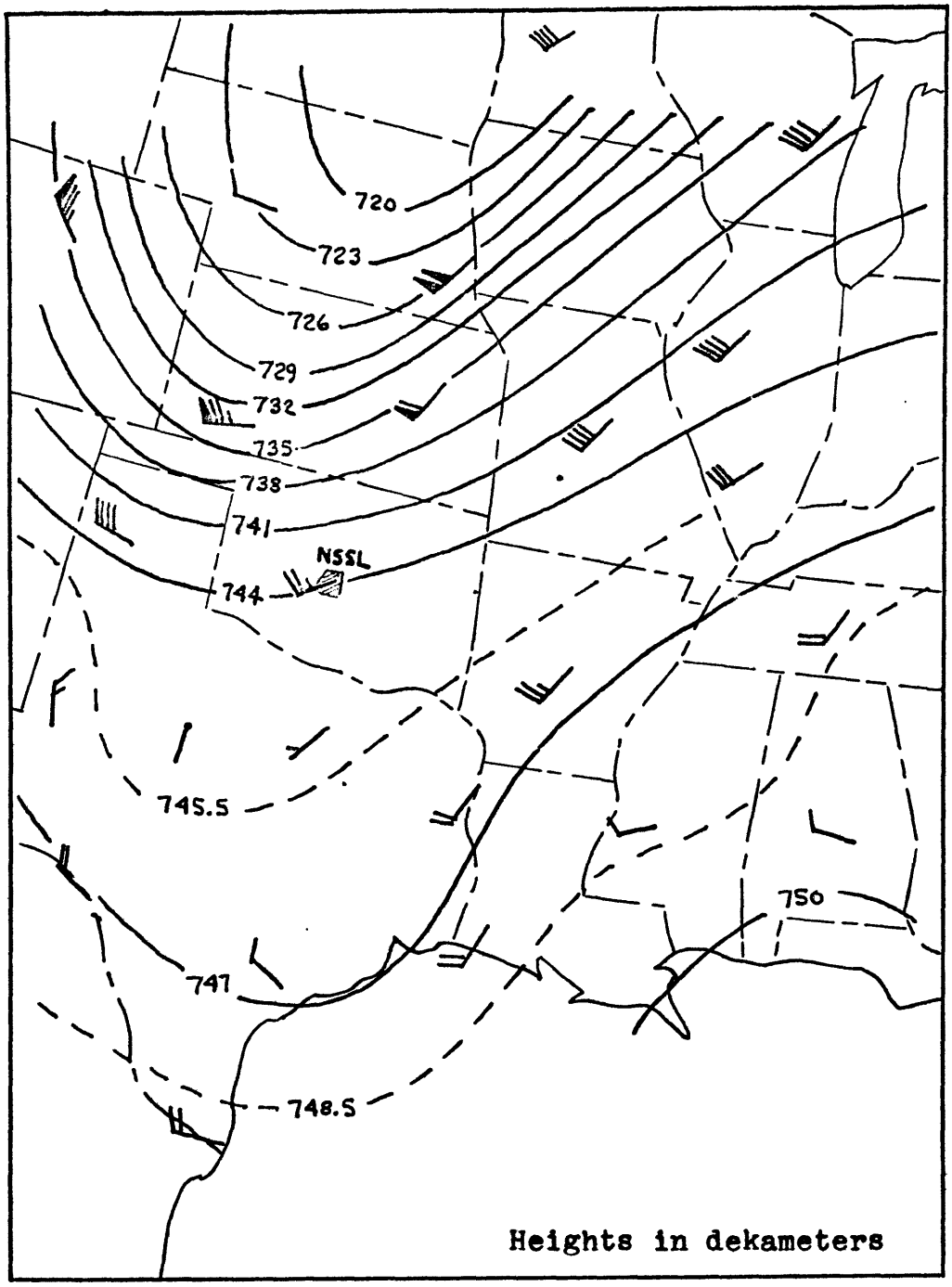

FIGURE 26 - The 400-mb Analysis at 0600 CST, 15 May 1970

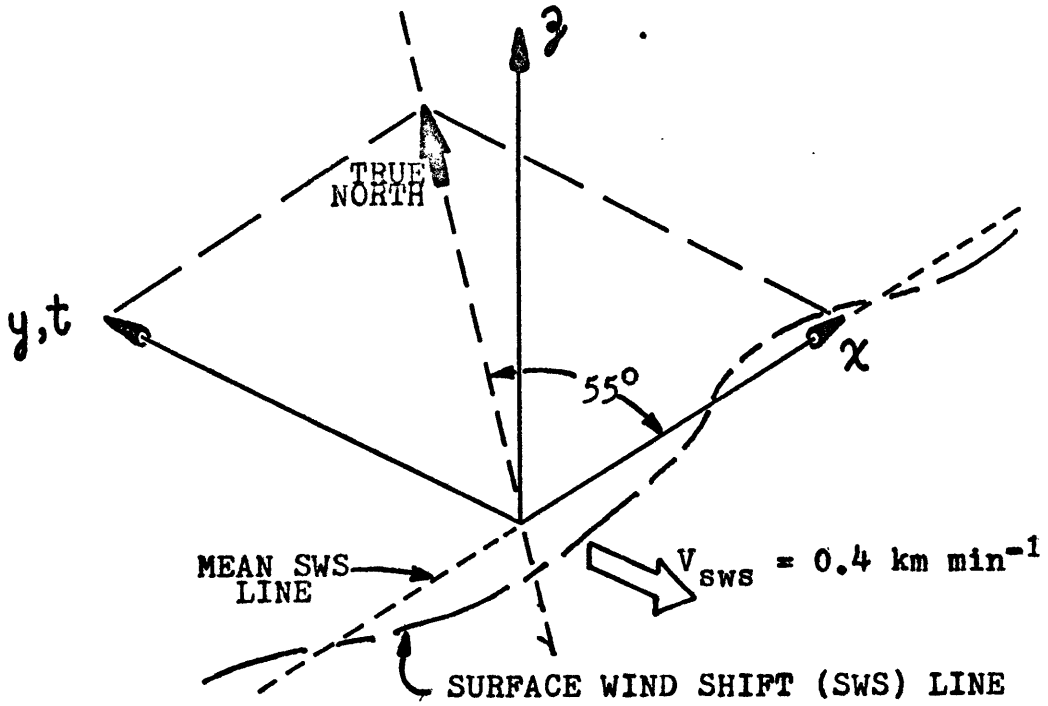

FIGURE 27 - Coordinate System

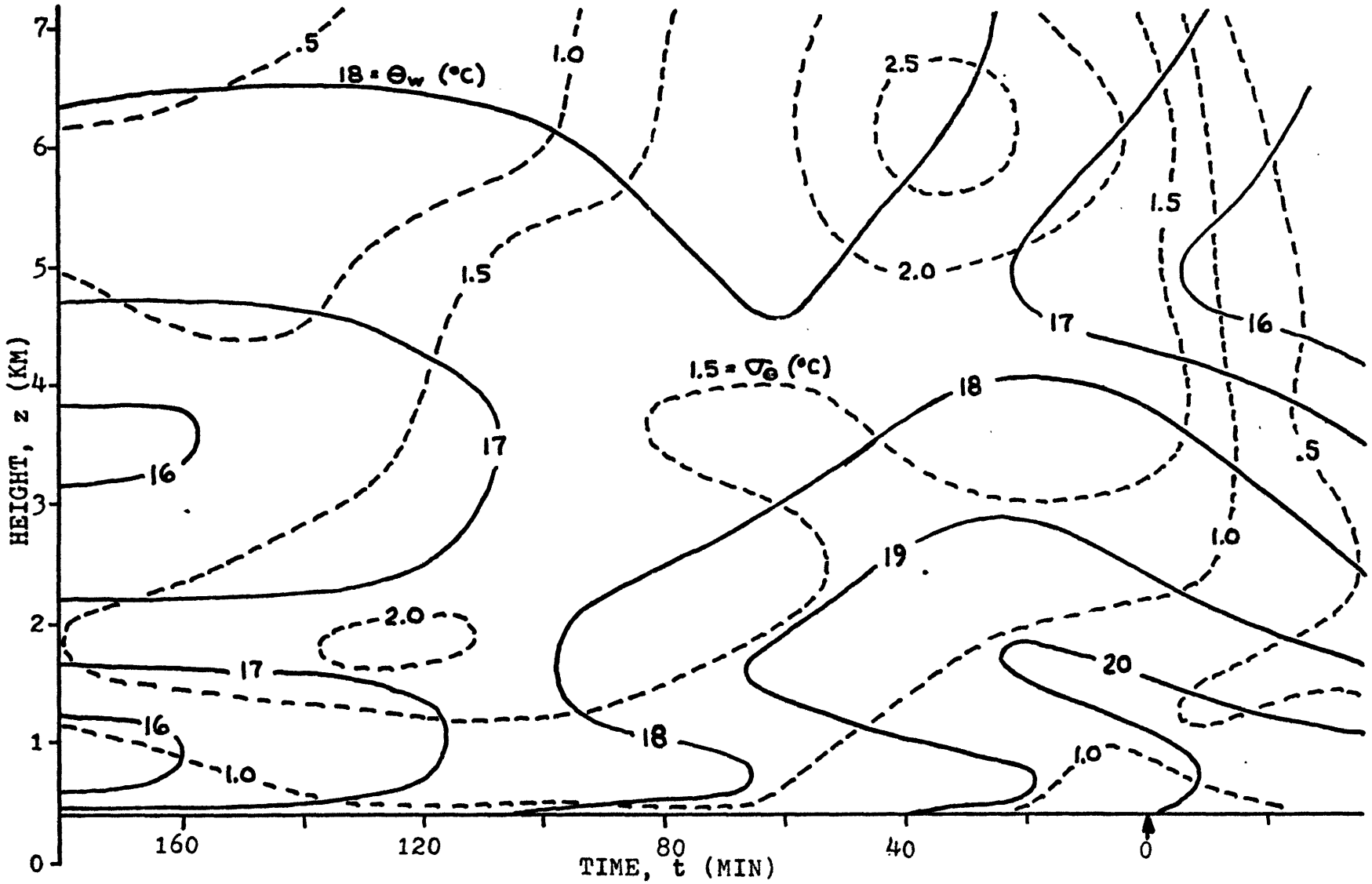

FIGURE 28 - Distribution of Wet-Bulb Potential Temperature, θ_w

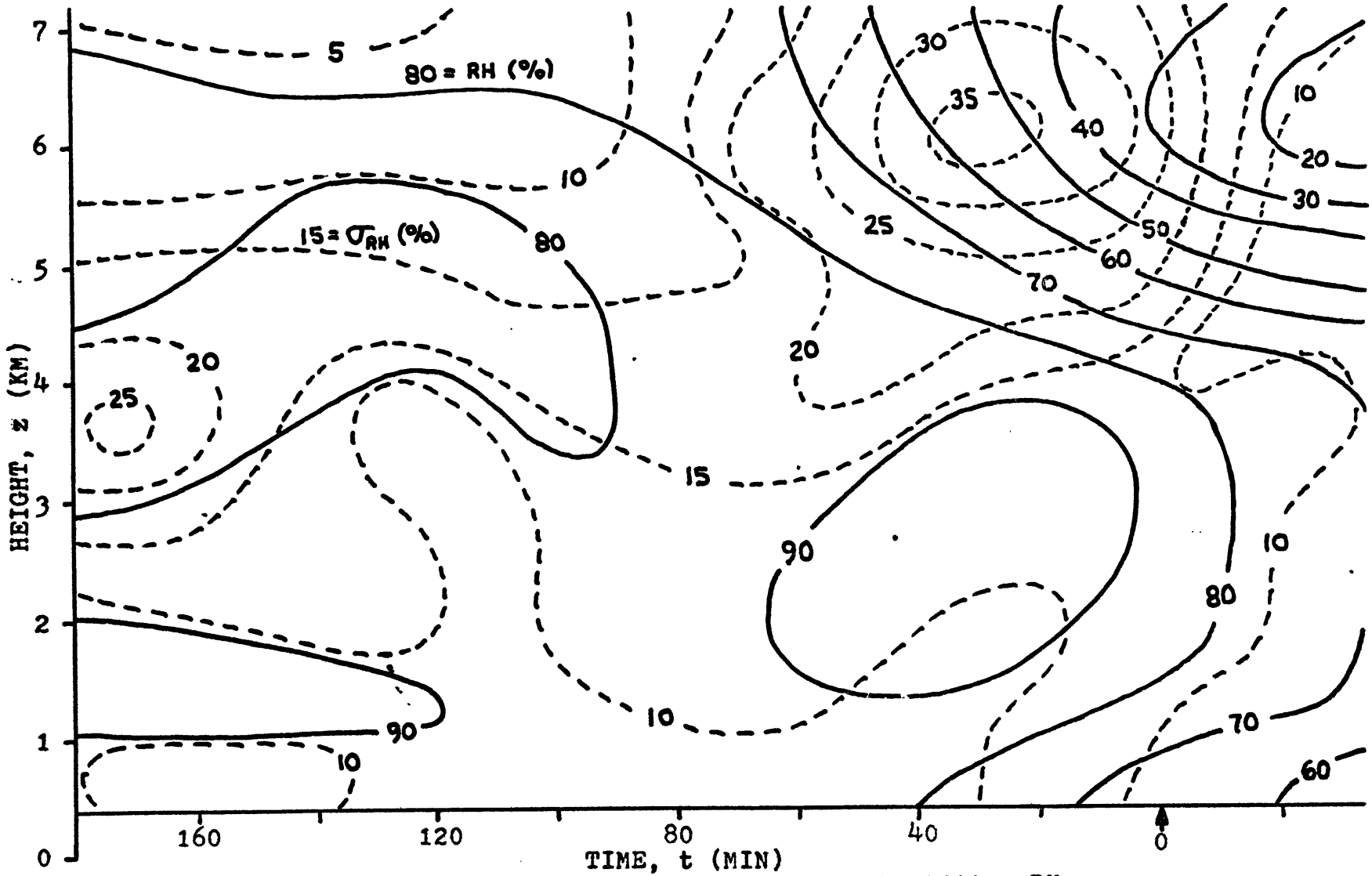

FIGURE 29 - Distribution of Relative Humidity, RH

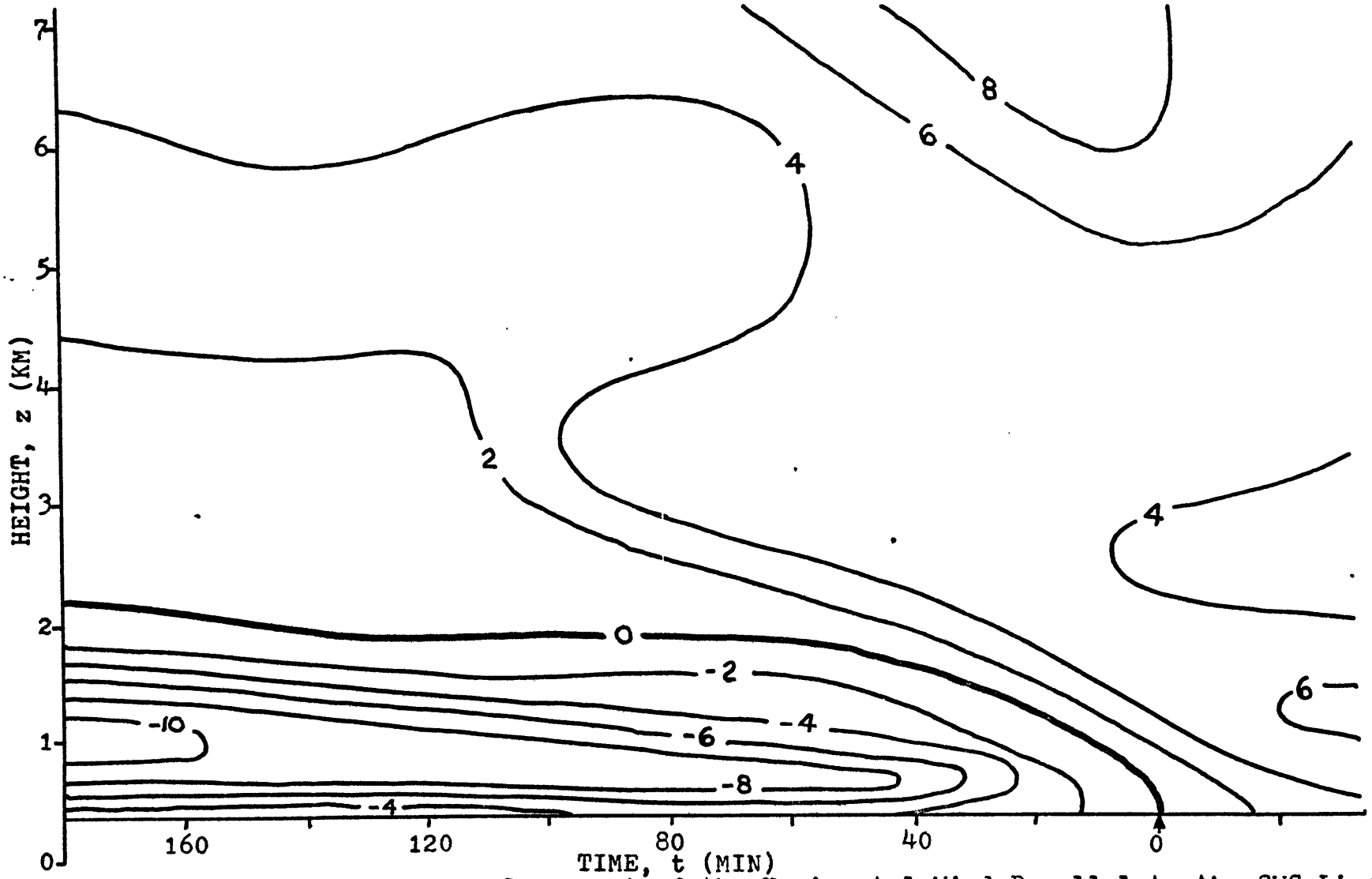

FIGURE 30 - Distribution of the Component of the Horizontal Wind Parallel to the SWS Line u (M SEC^{-1}) (Relative to Ground)

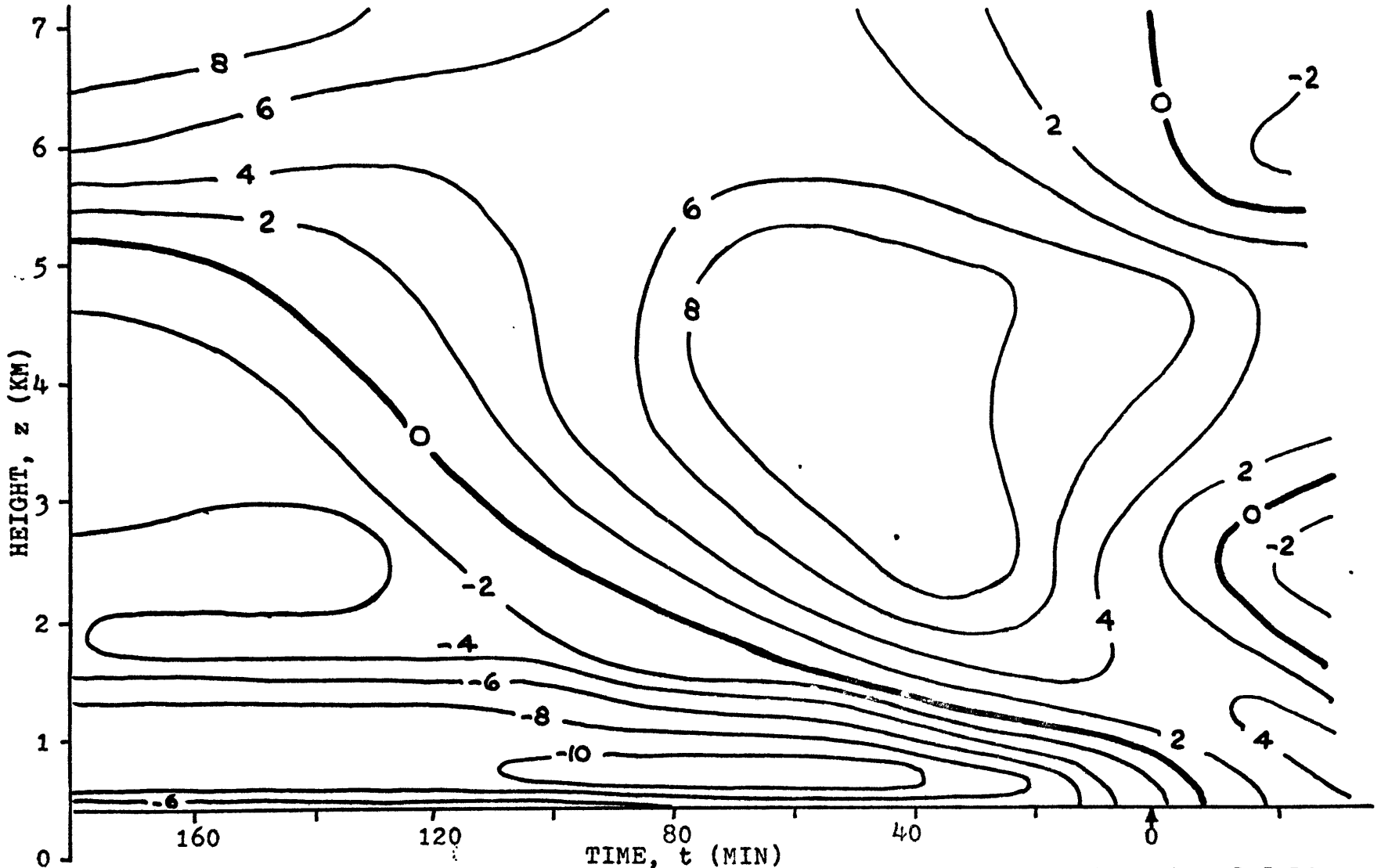

FIGURE 31 - Distribution of the Component of the Horizontal Wind Normal to the SWS Line v ($M\ SEC^{-1}$) (Relative to Ground)

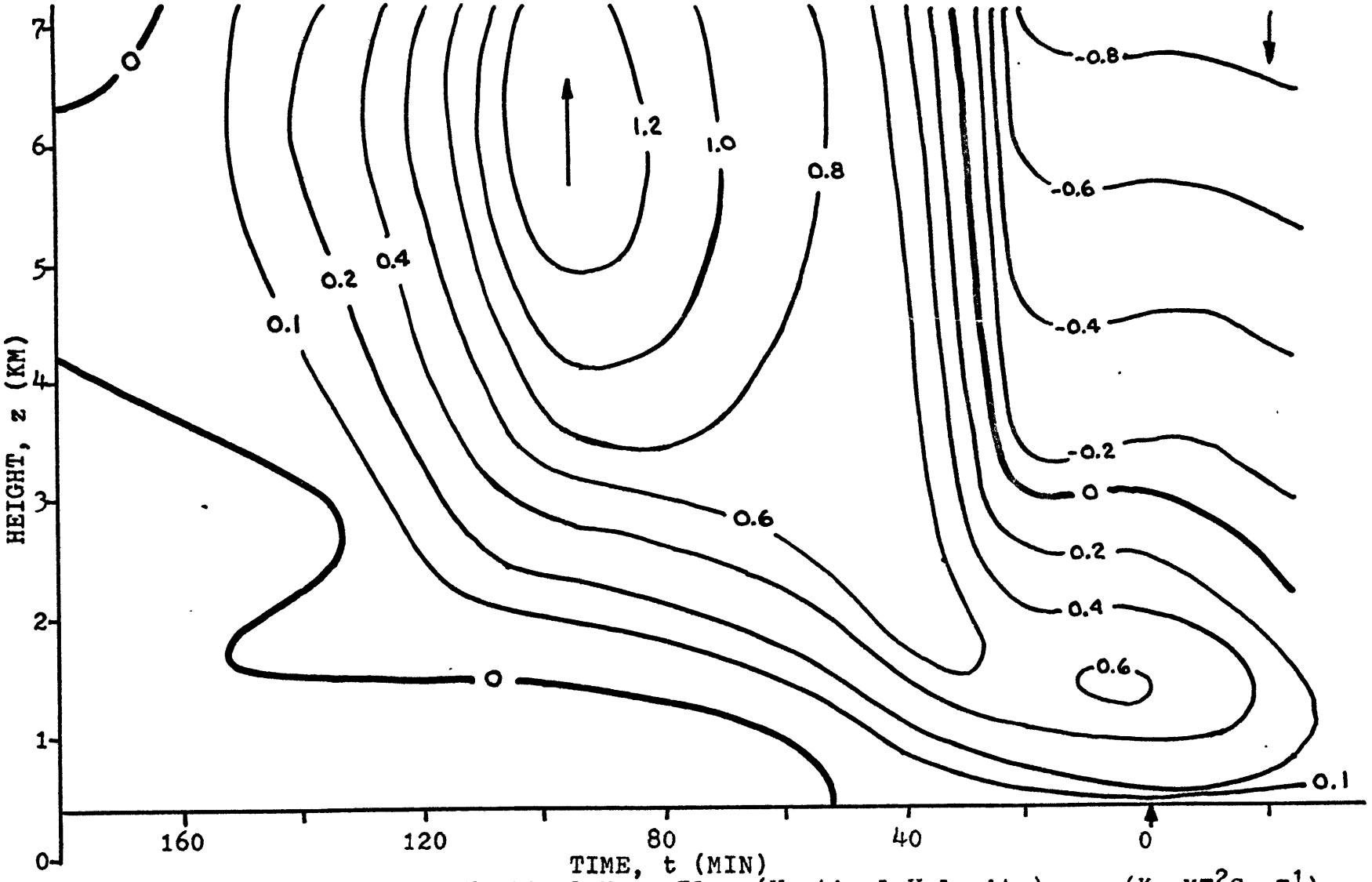

FIGURE 32 - Distribution of Vertical Mass Flux (Vertical Velocity), ρw (Kg $M^{-2}Sec^{-1}$)

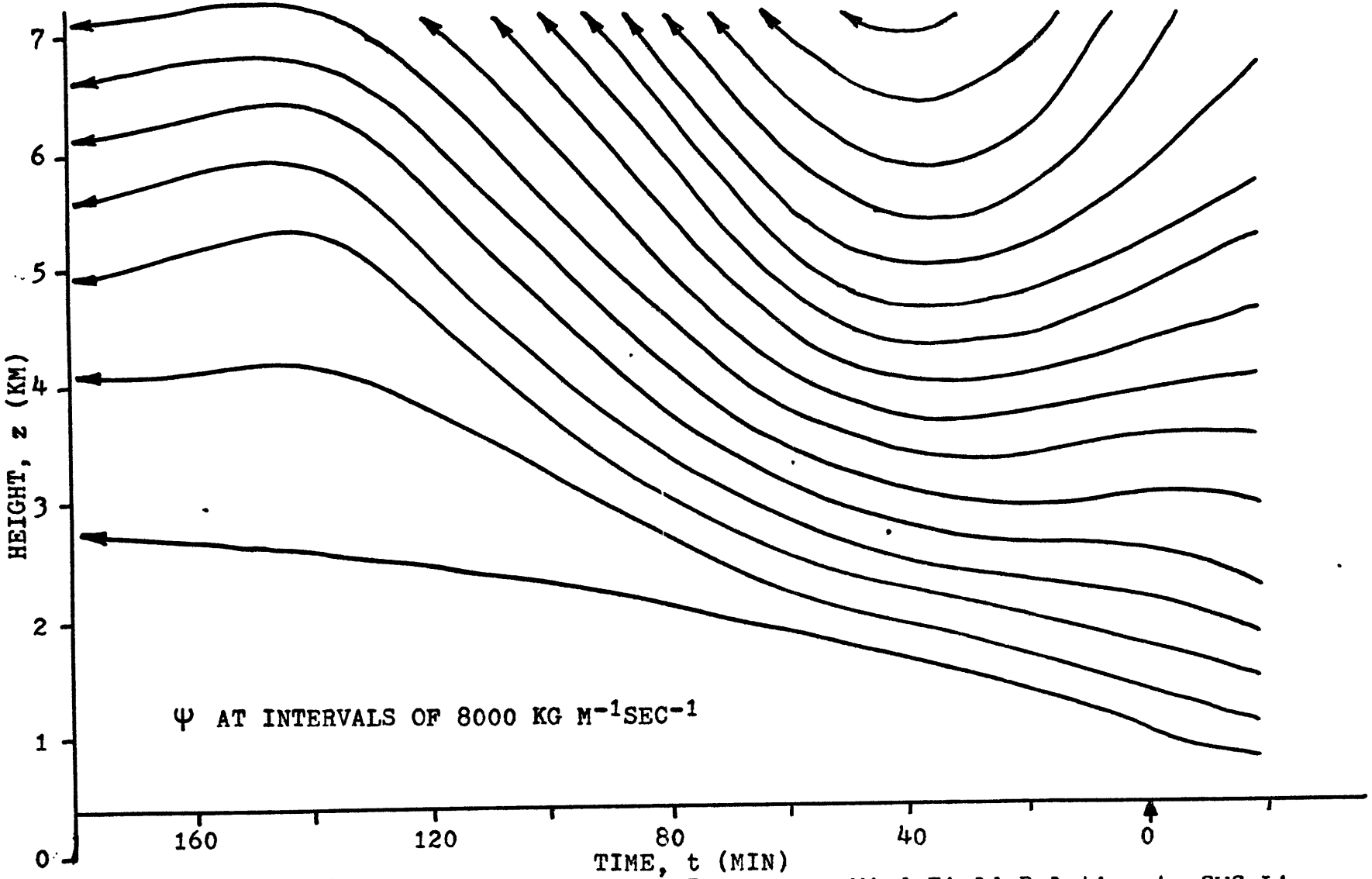

FIGURE 33 - Streamlines of the Mean Transverse Wind Field Relative to SWS Line

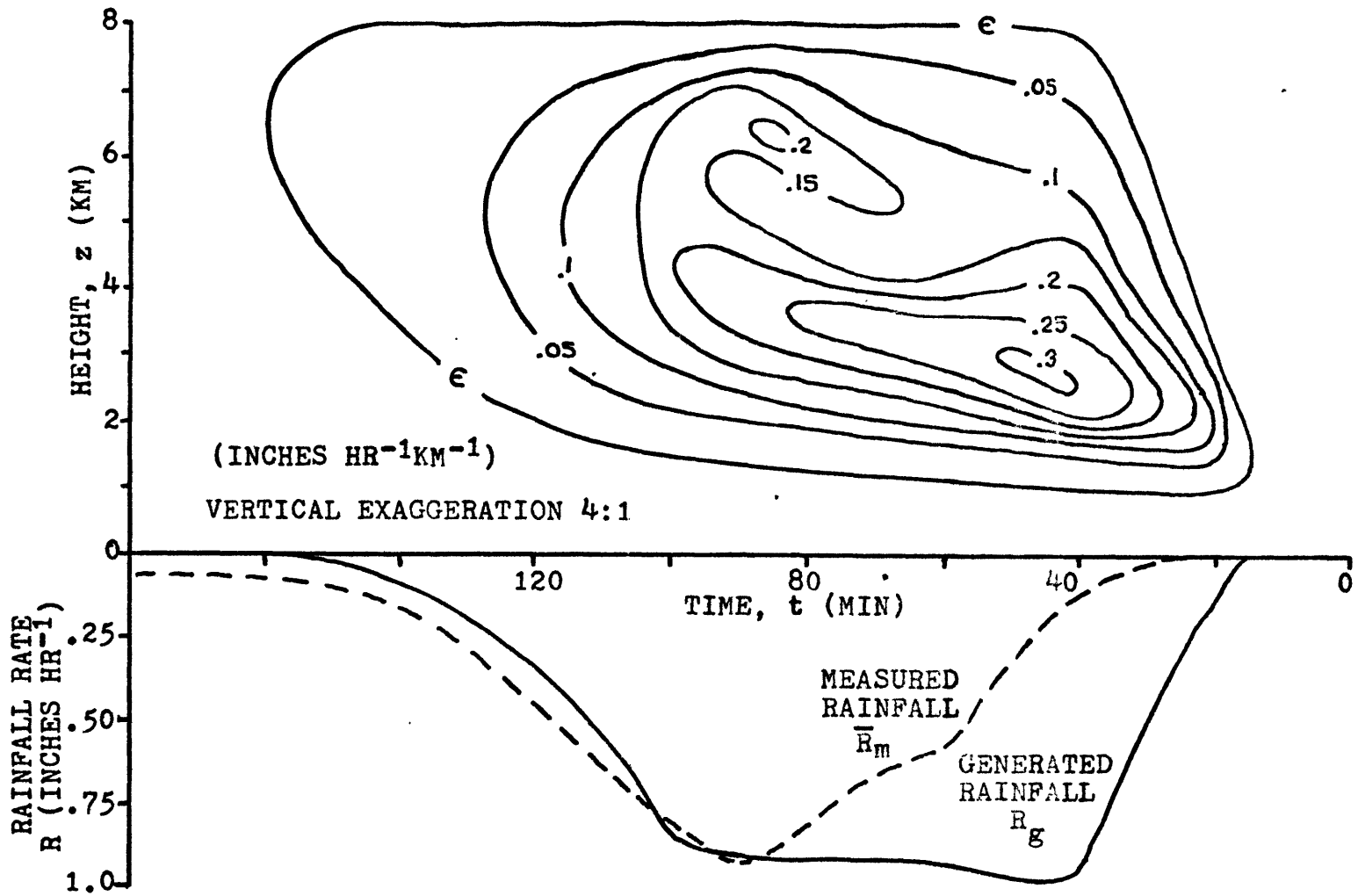

FIGURE 34 - Distribution of Liquid Water Generation and Comparison with Rainfall Rate

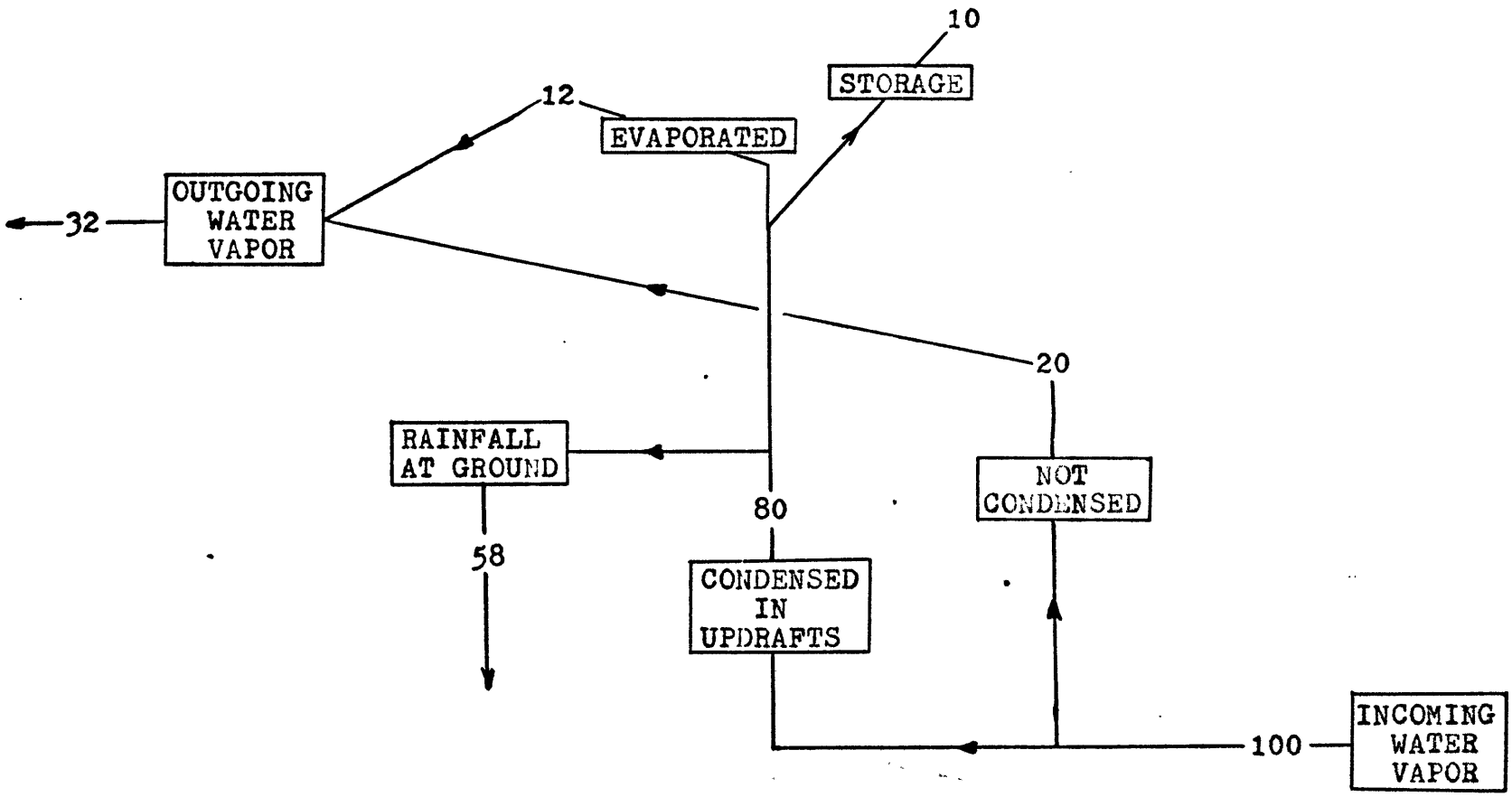

FIGURE 35 - Water Budget Diagram (Arbitrary Units)

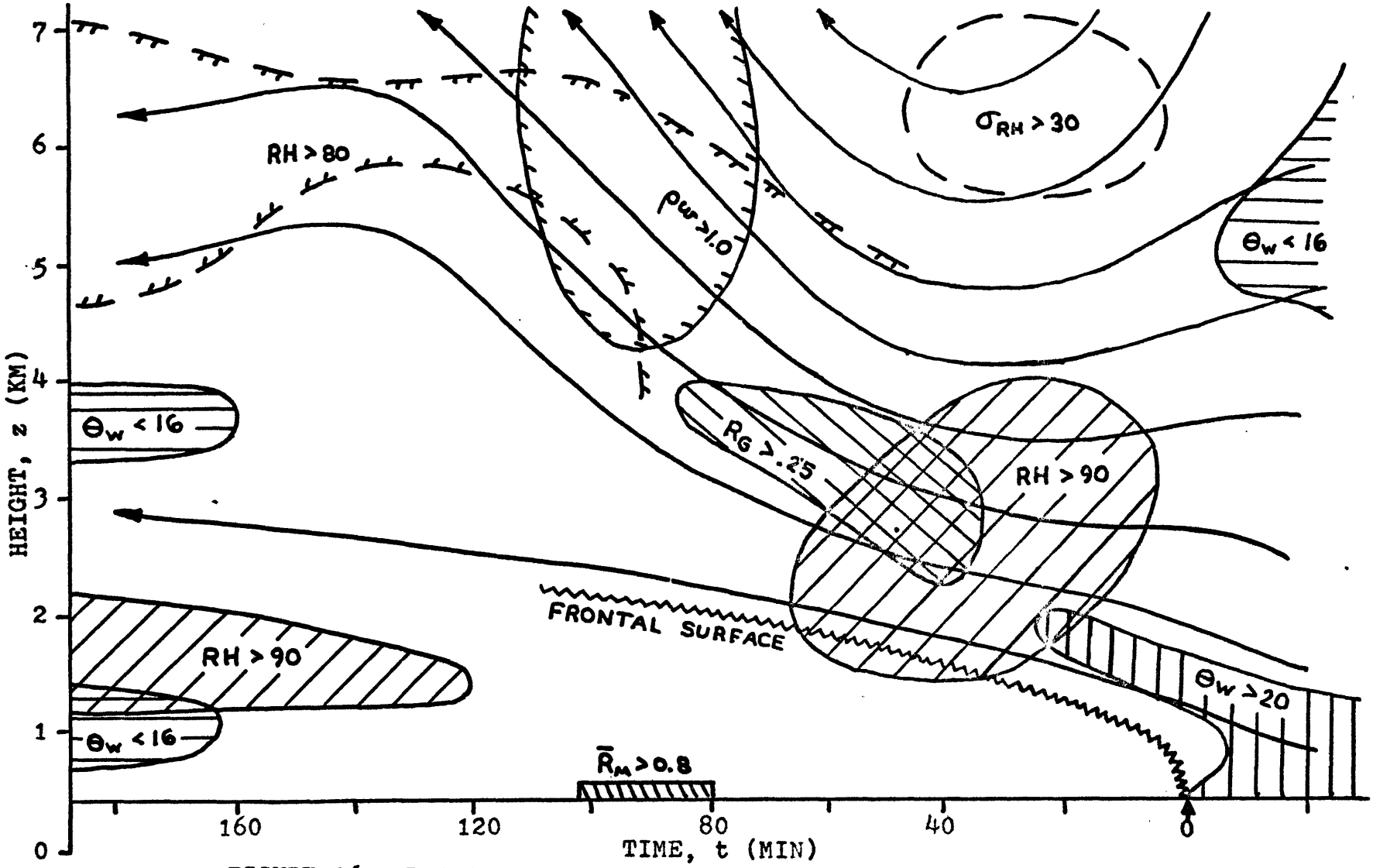

FIGURE 36 - Relationships Among the Meteorological Variables

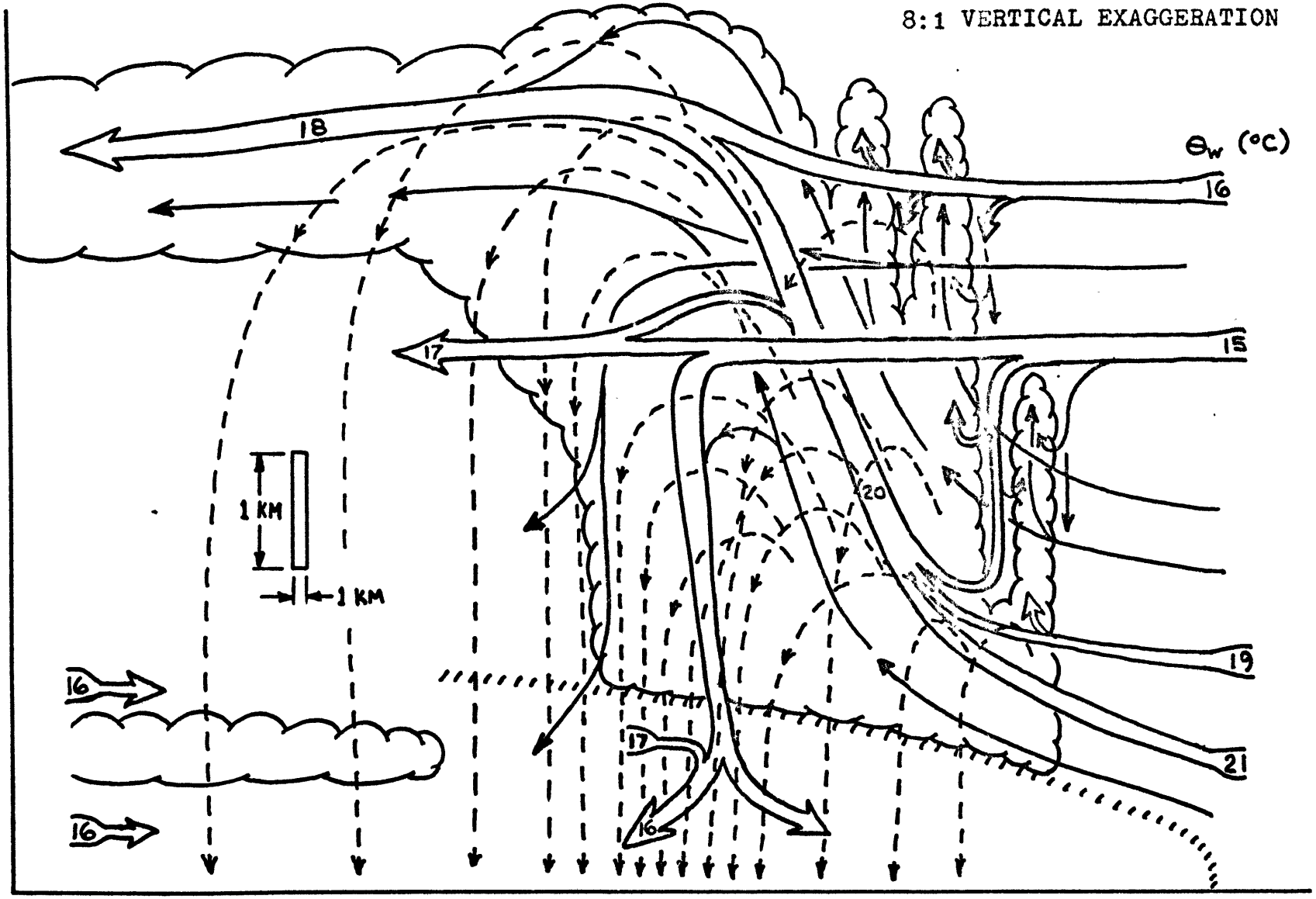

FIGURE 37 - Schematic Model of Storm System

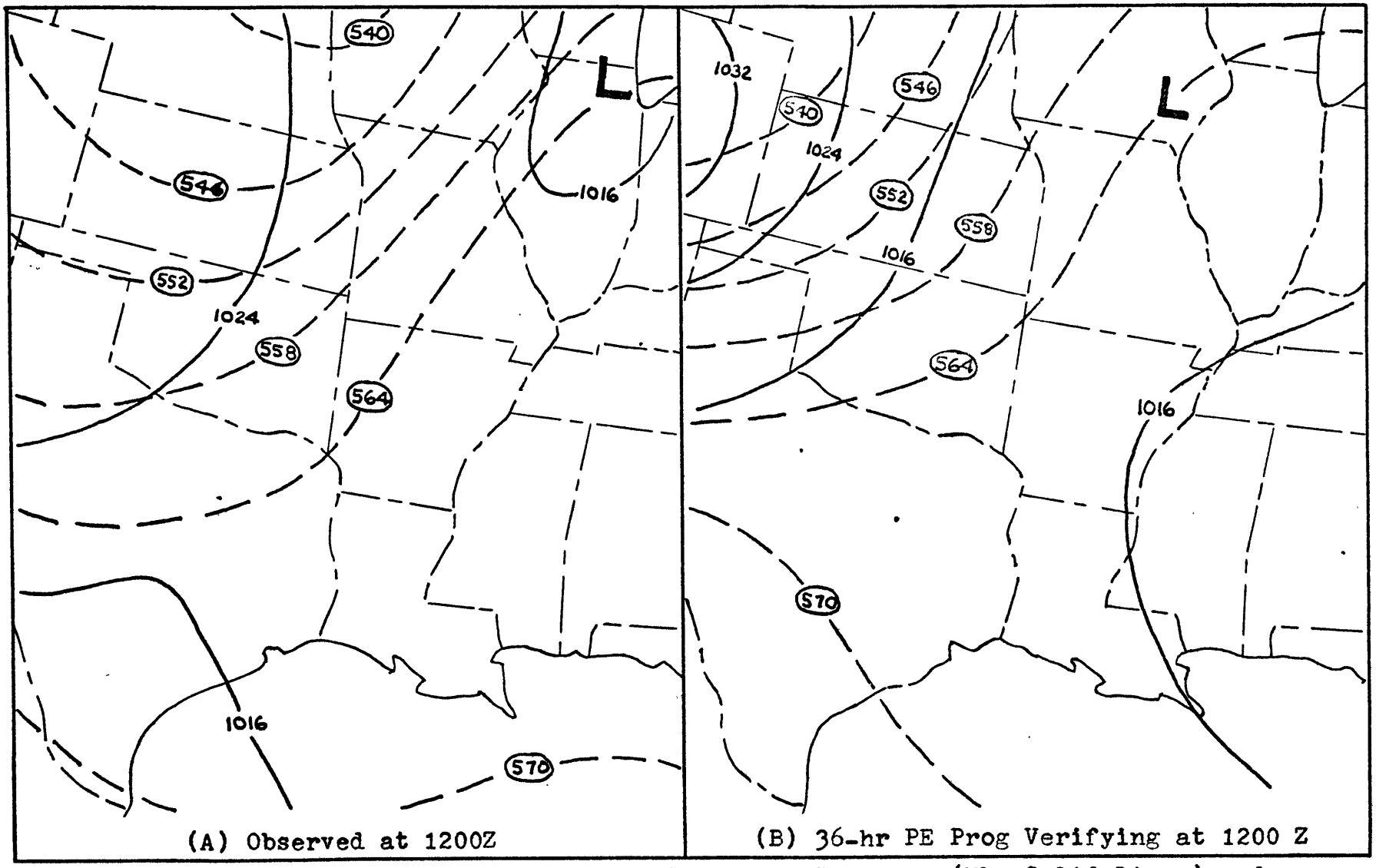

FIGURE 38 - Observed and Predicted Sea-Level Pressure (Mb, Solid Lines) and 1000-500 Mb Thickness (Dkm, Broken Lines) for 1200 Z, 15 May 1970

6. REFERENCES

Barnes, S.L., Henderson, J.H., and Ketchum, R.J. (1971), "Rawinsonde Observation and Processing Techniques at the National Severe Storms Laboratory," NOAA TM ERL NSSL-53, April 1971.

Browning, K.A. (1964), "Airflow and Precipitation Trajectories Within Severe Local Storms Which Travel to the Right of the Winds," Journal of the Atmospheric Sciences, Vol. 21, Nov. 1964, pp. 634-639.

Browning, K.A., and Ludlum, F.H. (1962), "Airflow in Convective Storms," Quarterly Journal of the Royal Meteorological Society, Vol. 88, April 1962, pp. 117-135.

Byers, H.R., and Braham, R.R.,Jr. (1949), The Thunderstorm: Report of the Thunderstorm Project, U.S. Air Force, U.S. Navy, U.S. Advisory Committee for Aeronautics, and U.S. Weather Bureau, June 1949.

Charba, J., and Sasaki, Y. (1968), "Structure and Movement of the Severe Thunderstorms of April 3, 1964 as Revealed from Radar and Surface Mesonetwork Data Analysis," ESSA TM ERL NSSL-41, October 1968.

Fankhauser, J.C. (1971), "Thunderstorm-Environment Interactions Determined From Aircraft and Radar Observations," Monthly Weather Review, Vol.99, March 1971, pp. 171-192.

Fujita, T., and Grandoso, H. (1968), "Split of a Thunderstorm Into Anticylonic and Cyclonic Storms and Their Motion as Determined From Numerical Model Experiments," Journal of the Atmospheric Sciences, Vol. 25, May 1968, pp. 416-439.

Galway, J.G. (1956), "The Lifted Index as a Predictor of Latent Instability," Bulletin of the American Meteorological Society, Vol. 37, Dec. 1956, pp. 528-529.

Hookings, G.A. (1965), "Precipitation-Maintained Downdrafts," Journal of Applied Meteorology, Vol. 4, April 1965, pp. 190-195.

Hoskins, B.J., and Bretherton, F.P. (1972), "Atmospheric Frontogenesis Models: Mathematical Formulation and Solution," Journal of the Atmospheric Sciences, Vol. 29, Jan. 1972, pp. 11-37.

Marwitz, J.D. (1972), "The Structure and Motion of Severe Hailstorms," Parts I,II, and III, Journal of Applied Meteorology, Vol. 11, Feb. 1972, pp. 166-201.

Newton, C.W., and Fankhauser, J.C. (1964), "On the Movements of Convective Storms, With Emphasis on Size Discrimination in Relation to Water-Budget Requirements," Journal of Applied Meteorology, Vol. 3, Dec. 1964, pp. 651-668.

Newton, C.W. and Newton, H.R. (1959), "Dynamical Interactions Between Large Convective Clouds and Environment With Vertical Shear," Journal of Meteorology, Vol. 16, Oct. 1959, pp. 483-496.

NSSL Operations Staff (1971), "The NSSL Surface Network and Observations of Hazardous Wind Gusts," NOAA TM ERL NSSL-55, June 1971.

Petterson, S. (1956), Weather Analysis and Forecasting: Volume I, Motion and Motion Systems, (2nd edition), McGraw-Hill Book Company, 1956.

Whitehead, D.R. (1971), "A Comparison of Objective Convective Activity Indices," University of Oklahoma Atmospheric Research Institute, OURI-1828-71-1, Nov. 1971.

ACKNOWLEDGEMENTS

I wish to thank Professor Sanders for suggesting the topic and to express my sincere appreciation for his discussions and helpful suggestions and particularly for the time he spent examining the rough draft. I wish also to thank Mr. J. T. Dooley of NSSL for providing the data.